



Available online at www.sciencedirect.com



The Indispensable N-Terminal Half of eIF3j/HCR1 Cooperates with its Structurally Conserved Binding Partner eIF3b/PRT1-RRM and with eIF1A in Stringent AUG Selection

Latifa ElAntak^{1†}, Susan Wagner^{2†}, Anna Herrmannová^{2†},
Martina Karásková², Edit Rutkai², Peter J. Lukavsky^{1*}
and Leoš Valášek^{2*}

¹Structural Studies Division,
MRC-Laboratory of Molecular
Biology, Hills Road, Cambridge
CB2 2QH, England, UK

²Laboratory of Regulation of
Gene Expression, Institute of
Microbiology AVCR, v.v.i.,
Videnska 1083, Prague 142 20,
Czech Republic

Received 16 October 2009;

received in revised form

17 December 2009;

accepted 22 December 2009

Available online

11 January 2010

Despite recent progress in our understanding of the numerous functions of individual subunits of eukaryotic translation initiation factor (eIF) 3, little is known on the molecular level. Using NMR spectroscopy, we determined the first solution structure of an interaction between eIF3 subunits. We revealed that a conserved tryptophan residue in the human eIF3j N-terminal acidic motif (NTA) is held in the helix α 1 and loop 5 hydrophobic pocket of the human eIF3b RNA recognition motif (RRM). Mutating the corresponding “pocket” residues in its yeast orthologue reduces cellular growth rate, eliminates eIF3j/HCR1 association with eIF3b/PRT1 *in vitro* and *in vivo*, affects 40S occupancy of eIF3, and produces a leaky scanning defect indicative of a deregulation of the AUG selection process. Unexpectedly, we found that the N-terminal half of eIF3j/HCR1 containing the NTA is indispensable and sufficient for wild-type growth of yeast cells. Furthermore, we demonstrate that deletion of either j/HCR1 or its N-terminal half only, or mutation of the key tryptophan residues results in the severe leaky scanning phenotype partially suppressible by overexpressed eIF1A, which is thought to stabilize properly formed preinitiation complexes at the correct start codon. These findings indicate that eIF3j/HCR1 remains associated with the scanning preinitiation complexes and does not dissociate from the small ribosomal subunit upon mRNA recruitment, as previously believed. Finally, we provide further support for earlier mapping of the ribosomal binding site for human eIF3j by identifying specific interactions of eIF3j/HCR1 with small ribosomal proteins RPS2 and RPS23 located in the vicinity of the mRNA entry channel. Taken together, we propose that eIF3j/HCR1 closely cooperates with the eIF3b/PRT1 RRM and eIF1A on the ribosome to ensure proper formation of the scanning-arrested conformation required for stringent AUG recognition.

© 2009 Elsevier Ltd. Open access under [CC BY license](#).

Edited by M. F. Summers

Keywords: translation initiation; AUG recognition; eIF3; eIF1A; NMR

*Corresponding authors. E-mail addresses: pjl@mrc-lmb.cam.ac.uk; valasekl@biomed.cas.cz.

† L.E., S.W., and A.H. contributed equally to this work.

Present address: L. ElAntak, CNRS-IBSM, Laboratoire Interactions et Modulateurs de réponses, 31, Chemin Joseph Aiguier, 13402 Marseille Cedex 20, France.

Abbreviations used: eIF, eukaryotic translation initiation factor; NTA, N-terminal acidic motif; GTP, guanosine-5'-triphosphate; Met-tRNA^{Met}, methionyl initiator tRNA; TC, ternary complex; MFC, multifactor complex; NTD, N-terminal domain; CTD, C-terminal domain; RRM, RNA recognition motif; cryo-EM, cryo-electron microscopy; hEIF3b, human eIF3b; hEIF3j, human eIF3j; RNP, ribonucleoprotein; wt, wild type; L5, loop 5; GST, glutathione S-transferase; Slg[−], slow growth; ORF, open reading frame; Gcn[−], general control nonderepressible; 3-AT, 3-aminotriazole; NOE, nuclear Overhauser enhancement; ITC, isothermal titration calorimetry; WCE, whole-cell extract; 3D, three-dimensional; 2D, two-dimensional; NOESY, NOE spectroscopy.

Introduction

Translation captures the transfer of genetic information stored in DNA into effector molecules (polypeptides). The efficiency and accuracy of the initiation phase of translation are masterminded by numerous proteins called eukaryotic translation initiation factors (eIFs). Among them, eIF2 associates in its guanosine-5'-triphosphate (GTP)-bound state with methionyl initiator tRNA (Met-tRNA_i^{Met}) to form a ternary complex (TC; eIF2/GTP/Met-tRNA_i^{Met}), which is subsequently recruited to the 40S small ribosomal subunit with the help of eIF1, eIF1A, eIF3, and eIF5, producing the 43S preinitiation complex (reviewed by Hinnebusch *et al.*¹ and Pestova *et al.*²). eIF1 and eIF1A serve to stabilize a conformation that opens the 40S-mRNA binding channel³ required for recruitment of mRNA, bound by the cap-binding complex eIF4F and poly(A) binding protein, in a reaction that is, at least in yeast, critically stimulated by eIF3.⁴ In the thus formed 48S preinitiation complex, the 40S subunit is believed to adopt an open/scanning-conductive conformation that enables inspection of successive triplets in the mRNA leader in an ATP-dependent process called scanning, which is relatively poorly understood. During this process, eIF5 stimulates partial GTP hydrolysis on eIF2, but the resultant P_i is not released until initiation codon-anti-codon base-pairing has induced a conformational switch to the closed/scanning-arrested form, accompanied by displacement of eIF1 (reviewed by Mitchell and Lorsch⁵). This irreversible reaction serves as the decisive rate-limiting step stalling the entire machinery, with the AUG start codon placed in the decoding center (P site) of the 40S subunit. eIF1 is responsible for preventing premature engagement with putative start codons, whereas eIF1A is believed to stabilize properly formed preinitiation complexes at the correct start codon. eIF3 also contributes to the latter process via its contacts with eIF1, eIF2, and eIF5; however, molecular details of its participation are not known.⁶ After eIF2 guanosine 5'-diphosphate release, the 60S large ribosomal subunit can join the 40S-mRNA-Met-tRNA_i^{Met} preinitiation complex in a reaction stimulated by a second GTPase, eIF5B. Subunit joining is thought to facilitate ejection of all eIFs, except for eIF1A⁷ and eIF3.⁸ When eIF5B guanosine 5'-diphosphate dissociates, the 80S initiation complex is ready for elongation.

eIF3 is the most complex initiation factor composed of six subunits in yeast *Saccharomyces cerevisiae* (a/TIF32, b/PRT1, c/NIP1, i/TIF34, g/TIF35, and j/HCR1), all of which have corresponding orthologues in mammalian eIF3 containing additional seven subunits (d, e, f, h, k, l, and m).⁹ Given such complexity, it is not surprising that eIF3 was demonstrated to promote nearly all initiation steps, including binding of TC and other eIFs to the 40S subunit, subsequent mRNA recruitment, and scanning for AUG recognition (reviewed by Hinnebusch⁹). These activities are facilitated by

other eIFs such as eIF2, eIF1, and eIF5, which make direct contacts with eIF3 and, at least in yeast, occur in the ribosome-free assembly called the multifactor complex (MFC).^{4,6,10–13} We previously pinpointed several eIF3 domains that could play a critical role in MFC association with the 40S subunit, including the N-terminal domain (NTD) and the C-terminal domain (CTD) of c/NIP1 and a/TIF32, and the RNA recognition motif (RRM) in the NTD of b/PRT1.^{12,14} Identification of direct interactions between the NTD of a/TIF32 and the small ribosomal protein RPS0A, and the CTD of a/TIF32 and helices 16–18 of 18S rRNA allowed us to propose that eIF3 associates with the solvent-exposed side of the small subunit¹⁴ (Fig. 1a), as suggested by others for mammalian eIF3.^{17,18} In support, we have recently demonstrated that a partial nonlethal deletion of the NTD of a/TIF32 significantly reduced the amounts of 40S-bound MFC components *in vivo*, implicating this domain in the formation of a critical intermolecular bridge between eIF3 and the 40S subunit.⁸

Whereas there is no structural information available on yeast eIF3, whose detailed subunit interaction map is well defined,¹⁰ the recent cryo-electron microscopy (cryo-EM) study of human eIF3 revealed a low-resolution particle with a five-lobed architecture.¹⁸ The first attempt to unveil details of the spatial arrangement of its subunits and interactions between them suggested that human eIF3 is composed of three relatively stable modules, one of which bears resemblance to the yeast eIF3 core complex.¹⁹ Both yeast and mammalian eIF3 were suggested to associate with the 40S subunit via its solvent-exposed side (Fig. 1a).^{8,14,18} We recently provided the first insight into the molecular nature of eIF3 subdomains by resolving the NMR solution structure of the RRM of human eIF3b (heIF3b).²⁰ We reported a noncanonical RRM with a negatively charged surface in the β -sheet area, contradictory to the potential RNA binding activity of typical RRMs. Instead, we found that human eIF3j (heIF3j) interacts with the basic area of heIF3b-RRM, opposite to its β -sheet surface, via its N-terminal 69-amino-acid peptide, and that this interaction promotes heIF3b-RRM recruitment to the 40S subunit.

eIF3b is considered to serve as the major scaffolding eIF3 subunit shown to interact with a, c, g, i, and j in both mammals and yeast,^{10,19,21–25} clearly illustrating a high evolutionary conservation of its structure-organizing role. Indeed, we previously demonstrated that b/PRT1 also interacts with j/HCR1 via its N-terminal RRM domain,²⁵ and this contact was later implicated in the ability of j/HCR1 to stimulate 40S binding by eIF3. Remarkably, mutating the ribonucleoprotein (RNP) 1 motif of b/PRT1-RRM in *bprt1-rnp1* was shown to modestly increase leaky scanning, suggesting that the RRM of b/PRT1 also contributes to the efficiency of AUG recognition.

j/HCR1 is the only nonessential subunit in yeast²⁶ that is believed to stimulate eIF3 binding to the 40S subunit¹² and to promote 40S ribosome biogenesis.²⁷ Consistently, *in vitro* experiments revealed that heIF3j can bind to the 40S subunit by itself and is required for

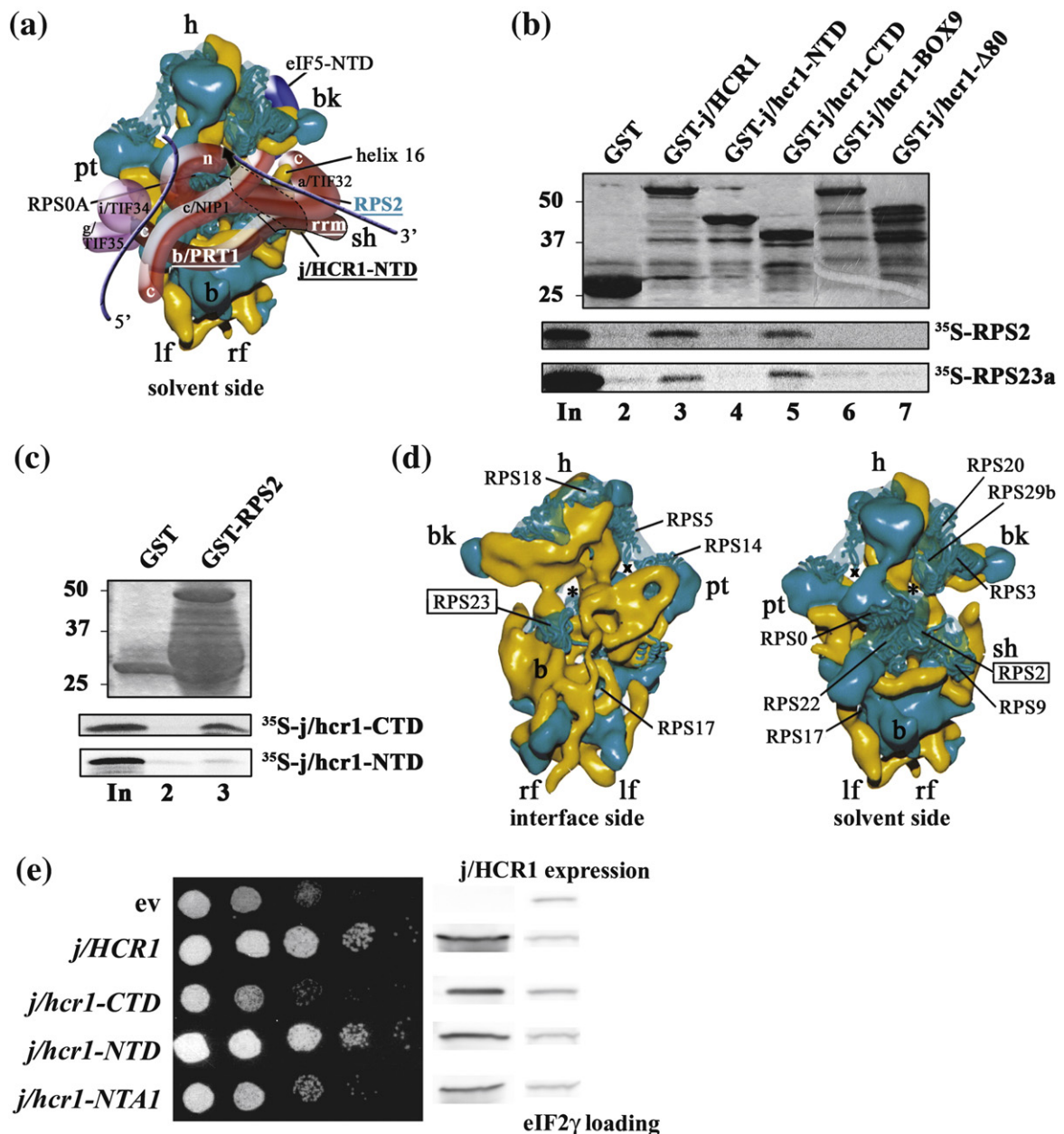


Fig. 1. The CTD of j/HCR1 interacts with RPS2 and RPS23a situated near the 40S mRNA entry channel, but is dispensable for efficient translation in yeast, as opposed to its NTD. (a) Hypothetical location of eIF3 on the solvent side of the *S. cerevisiae* 40S subunit based on cryo-EM reconstruction (adapted from Valášek *et al.*¹⁴). Protrusion of the CTD of eIF3j into the mRNA entry channel based on Fraser *et al.* is symbolized by a green arrow.¹⁵ Blue lines represent mRNA. (b and c) j/hcr1-CTD interacts with RPS2 and RPS23a via its KERR motif. (b) Full-length j/HCR1 (lane 3), its N-terminal half (lane 4) or C-terminal half (lane 5), various mutants (lanes 6 and 7) defined in Fig. 2b fused to GST, and GST alone (lane 2) were tested for binding against ³⁵S-labeled wt RPS2 and RPS23a; 10% of input amounts added to each reaction are shown in lane 1 (In). (c) RPS2 fused to GST (lane 3) and GST alone (lane 2) were tested for binding to ³⁵S-labeled j/hcr1-CTD and NTD essentially in the same manner as in (b). (d) Cryo-EM reconstruction of the *S. cerevisiae* 40S subunit (adapted from Spahn *et al.*¹⁶). The 40S subunit is shown from the interface side (left) or the solvent side (right), with RNA segments in yellow and with proteins in green. The mRNA entry and exit channels are designated by (*) and (X), respectively. (e) j/hcr1-NTD is required for wt growth dependent on its intact NTA. Transformants of H428 (j/hcr1Δ) bearing an empty vector, YEp-j/HCR1-DS, YEp-j/hcr1-CTD, YEp-j/hcr1-NTD, and YEp-j/hcr1-NTA1, respectively, were spotted in five serial 10-fold dilutions on SD medium and incubated at 30 °C for 1.5 days. The far-right columns contain the results of Western blot analysis of WCEs from the very same strains using anti-j/HCR1 (j/HCR1 expression) and anti-GCD11 (eIF2γ loading) antibodies, respectively.

the stable 40S association of purified eIF3.^{7,22,28} Intriguingly, heIF3j, in the absence of other factors, was also demonstrated to be mutually antagonistic

for binding to the 40S subunit with mRNA.^{7,15} Furthermore, mutual exclusivity for heIF3j in 40S subunit binding was also observed with eIF1A.¹⁵

These results, together with determination of the position of heIF3j-CTD in the 40S mRNA entry channel and in the ribosomal A site by hydroxyl radical probing,¹⁵ suggested that eIF3j may coordinate binding of mRNA and eIFs within the decoding center and thus perhaps influence transitions between scanning-conductive and scanning-arrested conformations. To gain a full understanding of the physiological roles of eIF3j, we obtained detailed biochemical and structural information of its interactions and examined their importance in living cells.

Unexpectedly, here we show that the NTD of j/HCR1 is indispensable and sufficient for wild-type (wt) growth. Strikingly, we also found that deletion of j/HCR1 (or its NTD only) leads to a strong leaky scanning phenotype indicative of a defect in AUG recognition, partially suppressible by increased gene dosage of eIF1A. These novel results strongly suggest that eIF3j remains bound to scanning ribosomes even after mRNA recruitment. NMR spectroscopic analysis revealed that heIF3j is held via its N-terminal acidic motif (NTA) centered by the conserved tryptophan (Trp52) in a hydrophobic pocket formed by helix α 1 and loop 5 (L5) of heIF3b-RRM. To our knowledge, this is the first structural insight into molecular interactions within eIF3 from any organism. Mutating these evolutionary conserved determinants in yeast j/HCR1 and b/PRT1 subunits disrupted their direct binding *in vitro*, as well as j/HCR1 association with MFC, but not with 40S subunits *in vivo*. Both j/HCR1 and b/PRT1 mutations resulted in growth phenotypes and imparted severe leaky scanning defects. The b/PRT1-RRM mutation then, in addition, strongly reduced the association of the core eIF3 with 40S subunits, suggesting that it forms, either directly or indirectly, an important intermolecular bridge between eIF3 and the small ribosomal subunit. We conclude that the key function of the NTD of j/HCR1 is to cooperate with the RRM of b/PRT1 and eIF1A on the 40S subunit to ensure proper establishment of the scanning-arrested conformation required for stringent AUG recognition.

Results

The N-terminal half of j/HCR1 is indispensable and sufficient for efficient translation in yeast

Recent observations made with glutathione S-transferase (GST) pull-down experiments showed that the last 16 amino acids of heIF3j are required for the stable binding of eIF3 to the 40S subunit,²² and that binding of heIF3j-CTD occurs in the 40S mRNA entry channel.¹⁵ Consistent with the latter, using GST pull-downs, we reproducibly detected weaker but highly specific interactions between the purified j/hcr1-CTD and small ribosomal proteins RPS2 and RPS23 (Fig. 1b, lane 5; Fig. 1c, middle panel) dependent on the last 80 amino acid residues of j/HCR1 and the intact KERR motif (K²⁰⁵- χ ₅-E²¹¹R²¹²- χ ₂-

R²¹⁵) (Fig. 1b, lanes 6 and 7), which is conserved between eIF3j and the HCR1-like domain of eIF3a across species (see the text below).²⁵ (None of the remaining small ribosomal proteins, whose location on the ribosome was predicted based on homology modeling with bacterial proteins, interacted with j/HCR1 in this assay.) RPS2 and RPS23 were previously shown to occur on the solvent and interface sides of the mRNA entry channel, respectively¹⁶ (Fig. 1d). Together, these findings suggest that the ribosomal binding site of the CTD of eIF3j might have remained evolutionary conserved and that it thus represents an important functional domain of eIF3j.

To examine this possibility, we first expressed the NTD and CTD of j/HCR1 (defined in Fig. 6b) in the j/hcr1 Δ strain and tested the resulting transformants for the suppression of its slow-growth (Slg⁻) phenotype. Surprisingly, we found that the CTD of j/HCR1 is dispensable for the wt growth of yeast cells in contrast to its NTD, the deletion of which phenocopied the Slg⁻ phenotype of j/HCR1 deletion (Fig. 1e, fourth row *versus* third row). [Both truncated proteins, as well as other j/HCR1 mutants mentioned below, had to be tested from high-copy vectors due to their decreased stability. In this arrangement, their expression levels were about 3-fold higher than the physiological level and similar to the level of overexpressed wt j/HCR1, which does not produce any phenotype (Fig. 1e; data not shown).] This finding implies that the NTD of j/HCR1 should be able to associate with the 40S subunit independently of its CTD. To test this, we employed a formaldehyde cross-linking method, followed by resedimentation of the 40S fractions on a second gradient, to minimize the trailing of non-cross-linked factors into 40S fractions. It is worth mentioning that this method provides the best available approximation of the native 43S/48S preinitiation complexes composition *in vivo*.²⁹ As shown in Fig. 2a–c, both j/hcr1-NTD and j/hcr1-CTD retained ~20% of wt affinity for the 40S subunit. (Bands in the upper fractions after resedimentation most likely represent j/HCR1 proteins not properly cross-linked to preinitiation complexes *in vivo* that dropped off during two consecutive high-velocity centrifugations.) When the nonequilibrium character of this assay is taken into account, the given percentages are only relative numbers and, in principle, suggest that both j/HCR1 halves show less stable binding to 40S subunits under these conditions than the full-length protein. In fact, since j/hcr1-NTD fully supports the growth of j/hcr1 Δ cells, it seems likely that in living cells, it associates with 40S subunits more efficiently. To learn whether the j/hcr1-NTD–40S interaction is bridged by eIF3, we examined the 40S binding of j/hcr1-NTD bearing a specific NTA1 mutation, which, as described in detail below, destroys direct j/HCR1–b/PRT1 interaction and completely diminishes j/HCR1 association with MFC *in vivo* (Figs. 6c and 7b). As shown in Fig. 2d, the j/hcr1-NTD-NTA1 mutant still associated with 40S subunits, albeit with an affinity reduced by ~30% compared to j/hcr1-NTD.

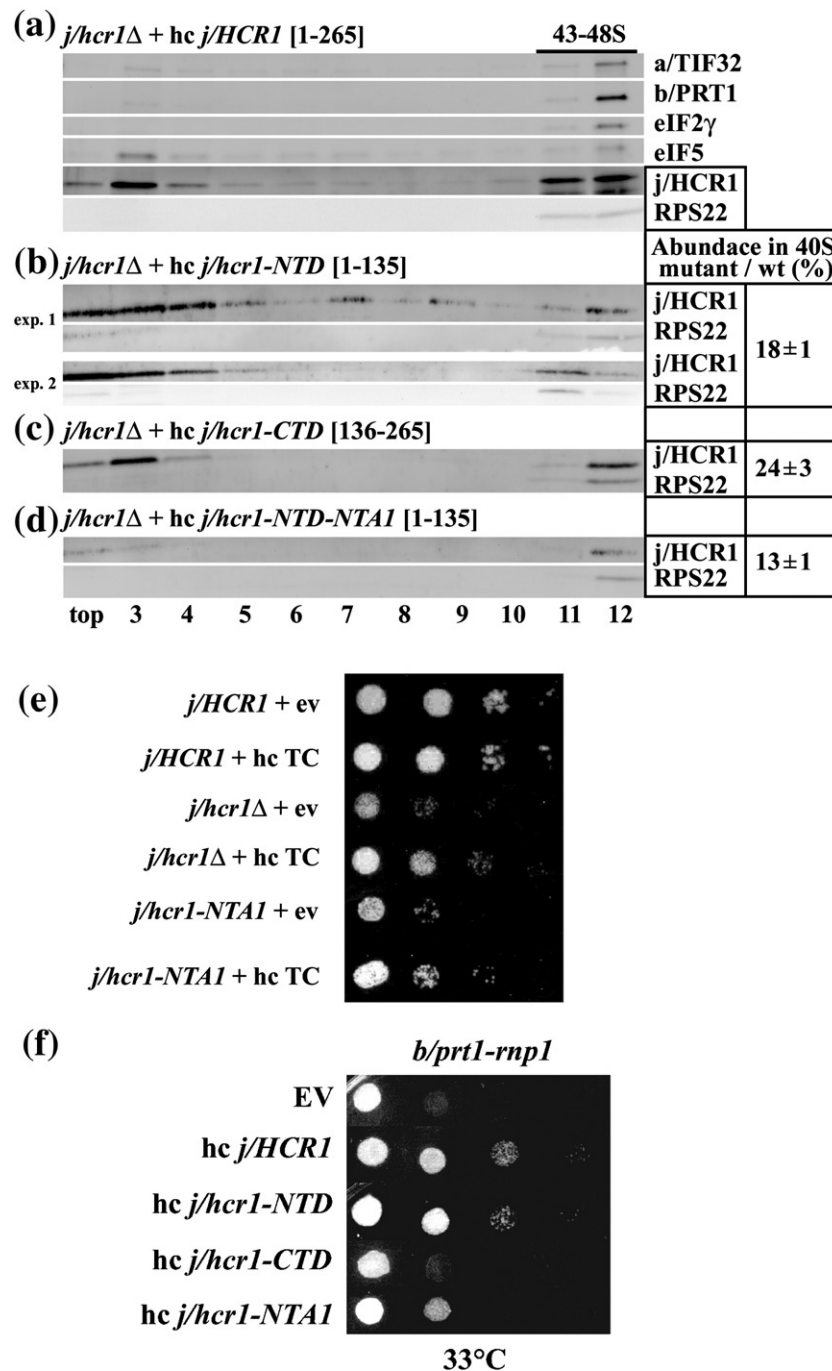


Fig. 2. Both the NTD and the CTD of j/HCR1 retain intrinsic 40S binding affinity. (a–d) Transformants of strain H428 (*j/hcr1Δ*) bearing YEp-j/HCR1-DS, YEp-j/hcr1-NTD, YEp-j/hcr1-CTD, and YEp-j/hcr1-NTD-NTA1, respectively, were grown in SD medium at 30 °C to an OD₆₀₀ of ~1.5 and cross-linked with 2% HCHO prior to harvesting. WCEs were prepared and subsequently separated on a 7.5–30% sucrose gradient by centrifugation at 41,000 rpm for 5 h. The 40S fractions were pooled, resolved on a second gradient, and subjected to Western blot analysis. The first two fractions were combined (top). Proportions of the 40S-bound j/HCR1 proteins relative to the amount of 40S subunits were calculated, using NIH ImageJ, from two independent experiments. The resulting values obtained with the wt strain were set to 100%, and those obtained with mutant strains were expressed as percentages of wt (SD given). (e–f) Genetic evidence that j/HCR1 with intact NTA (or only its NTD) stimulates 40S binding by eIF3. (e) Overexpression of TC partially suppresses the Slg[−] phenotype of *j/hcr1Δ* and *j/hcr1-NTA1* mutants. H416 (*j/HCR1*; rows 1 and 2), H428 (*j/hcr1Δ* YEplac181; rows 3 and 4), and SY73 (*j/hcr1Δ* YEp-j/hcr1-NTA1; rows 5 and 6) were transformed with either the empty vector (rows 1, 3, and 5) or the TC-overexpressing vector (rows 2, 4, and 6), and the resulting transformants were spotted in four serial 10-fold dilutions on SD medium and incubated at 30 °C for 2 days. (f) j/HCR1 with intact NTA (or only its NTD) partially suppresses the temperature-sensitive (Ts[−]) phenotype of *b/prt1-rnp1*. Transformants of the strain H3674 (*b/prt1-rnp1*)¹² bearing the empty vector, YEp-j/HCR1-DS, YEp-j/hcr1-NTD, YEp-j/hcr1-CTD, and YEp-j/hcr1-NTA1, respectively, were spotted in four serial 10-fold dilutions on SD medium and incubated at 33 °C for 3 days.

Together, these experiments indicate that both halves of j/HCR1 possess an intrinsic 40S binding affinity that is additive and further strengthened by j/HCR1 contacts with 40S-bound eIF3.

Deletion of *j/HCR1* was previously shown to reduce the amounts of 40S-bound eIF3.¹² We next wished to show that the wt-like-behaving *j/hcr1*-NTD is also fully capable of supporting eIF3 loading onto the 40S subunit. However, the differences in the amounts of eIFs associated with 40S subunits between wt and *j/hcr1Δ* cells were somewhat smaller in our hands than those observed in the previous study. Because this discrepancy is still under examination, we could not conclusively address this question here. Nevertheless, we made two genetic observations supporting the idea that at least part of the *j/hcr1Δ* growth defect could be associated with the reduced eIF3 binding to the 40S subunit and that *j/hcr1*-NTD can fully substitute for full-length j/HCR1 in this respect: (i) overexpression of all three eIF2 subunits and tRNA_i^{Met} (hc TC), previously shown to stimulate j/HCR1-independent 40S binding of eIF3,^{4,12} partially suppressed the Slg[−] phenotype of *j/hcr1Δ* cells (Fig. 2e, fourth row *versus* third row); and (ii) overexpression of *j/hcr1*-NTD, but not *j/hcr1*-CTD, suppressed the Slg[−] phenotype of the *b/prt1-rnp1* mutant to the same degree as full-length wt j/HCR1 (Fig. 2f, rows 3 and 4). *b/prt1-rnp1* mutation was previously shown to affect eIF3 binding to the 40S subunit in a manner that is partially suppressible by high-copy j/HCR1 (see also the text below).¹² Interestingly, J. Lorsch and colleagues also did not observe any effect of an increased binding of eIF3 (containing only trace amounts of endogenous j/HCR1) to 43S complexes by addition of saturating amounts of separately purified j/HCR1 *in vitro* (J. Lorsch, personal communication, 2009). Taken together, this suggests that, in yeast, the effect of j/HCR1 on the binding of the rest of eIF3 to 40S subunits may be more subtle than was believed.

Genetic evidence that the NTD of j/HCR1 promotes proper selection of the AUG start codon in cooperation with eIF1A

The fact that heIF3j was suggested to govern access to the mRNA entry channel and to influence mRNA–40S subunit association during scanning and AUG recognition¹⁵ prompted us to examine the stringency of AUG selection in *j/hcr1Δ* cells. We were interested mainly in assaying a leaky scanning defect that might suggest that the scanning preinitiation complexes have a reduced ability to switch from scanning-conductive conformation to scanning-arrested conformation when the start codon enters the P site.³⁰

To investigate this, we took advantage of a reinitiation mechanism of *GCN4* translational control that can be used as an experimental tool to monitor various translational steps. Translation of *GCN4* mRNA is repressed in nutrient-replete cells by the last three of a total of four short upstream open reading frames (ORFs) in its leader. Under starvation conditions, the concentration of TC is

reduced; as a result, a fraction of 40S subunits scanning downstream after terminating at the first reinitiation-permissive uORF1 rebinds TC only after bypassing inhibitory uORF2–uORF4 and then reinitiates at *GCN4*.³¹ Leaky scanning leads to skipping over the AUG of uORF1 by scanning ribosomes, which subsequently initiate at downstream-inhibitory uORFs, preventing cells from derepressing *GCN4* translation under starvation conditions. This is called the general control nonderepressible (*Gcn*[−]) phenotype and is characterized by the sensitivity of mutant cells to 3-aminotriazole (3-AT), an inhibitor of the *HIS3* product.

We found that *j/hcr1Δ GCN2*⁺ cells exhibit significant sensitivity to 3-AT (Fig. 3a, row 3), which was further illustrated by an ~50% reduction in the derepression of the wt *GCN4-lacZ* reporter in response to 3-AT compared to wt *j/HCR1*⁺ (Fig. 3b, “+”). Strikingly, examination of a *GCN4-lacZ* construct in which uORF1 is elongated and overlaps the beginning of *GCN4* revealed an ~8-fold increase in *GCN4-lacZ* expression in *j/hcr1Δ* cells (Fig. 3c, column 2). Similarly, an ~6-fold increase in *GCN4-lacZ* expression was also detected from a construct containing solitary uORF4 (Fig. 3d, column 2) that allows only a negligible level of reinitiation.^{8,32} These results thus strongly suggest that deletion of *j/HCR1* impairs *GCN4* translational control by allowing a large fraction of preinitiation complexes scanning from the cap to leaky scan at the AUG of uORF1. Furthermore, the cells expressing the NTD-less *j/hcr1*-CTD also displayed 3-AT sensitivity (Fig. 3a, row 5) and increased *GCN4-lacZ* expression with constructs monitoring leaky scanning (Fig. 3c and d, column 3) by ~7-fold, as opposed to those expressing the CTD-less *j/hcr1*-NTD that increased leaky scanning only by a small margin (Fig. 3d, column 4). Hence, these results clearly suggest that the NTD is, for the most part, responsible for the j/HCR1 contribution to the stringent AUG selection.

eIF1A was shown to functionally interact with heIF3j¹⁵ and is thought to facilitate pausing of the scanning preinitiation complexes at the correct start codon long enough to proceed with downstream initiation events—in other words, to prevent leaky scanning.^{5,30} Accordingly, we observed that overexpression of eIF1A partially suppressed both Slg[−] and *Gcn*[−] phenotypes of *j/hcr1Δ* (Fig. 3f, row 2) and, most importantly, reduced leaky scanning over uORF4 by ~50% (Fig. 3e, last column). Taken together, we propose that the NTD of j/HCR1 communicates with eIF1A during scanning and promotes the eIF1A role in inducing smooth transition to closed/scanning-arrested conformation upon AUG recognition.

The overall structure of the heIF3b-RRM_{170–274}–heIF3j_{35–69} complex

To gain a deeper insight into the collaboration between the j subunit and the b subunit of eIF3, we determined the solution structure of heIF3b-

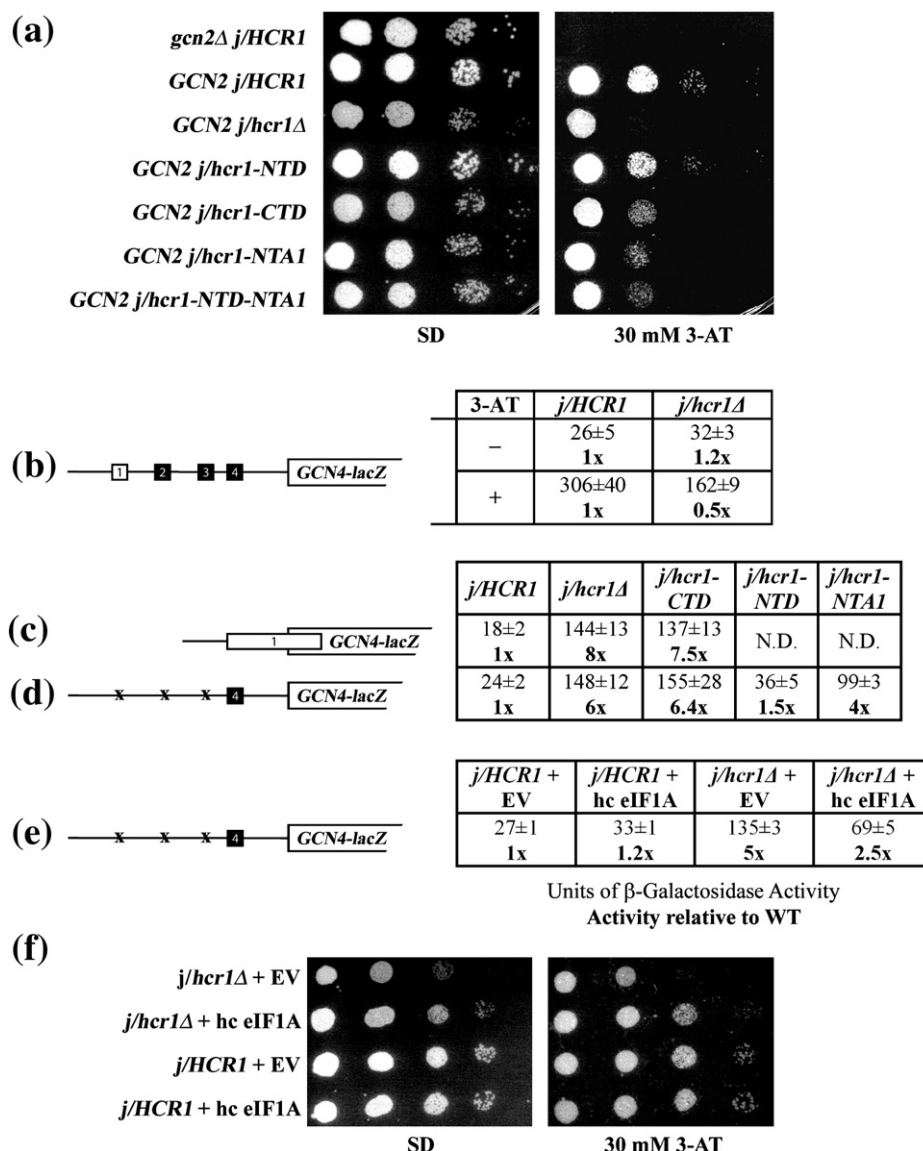


Fig. 3. Genetic evidence that the deletion of *j/hcr1*-NTD (or the *NTA1* mutation) prevents derepression of *GCN4* translation during starvation as a result of leaky scanning that is partially suppressible by high-copy eIF1A. (a) *j/hcr1Δ* imparts a *Gcn⁻* phenotype implicating *j/HCR1* in *GCN4* translational control. H418 (*gcn2Δ j/HCR1*; row 1) and H428 (*GCN2 j/hcr1Δ*) transformants bearing YEp-*j/HCR1* (row 2), YEplac181 (row 3), YEp-*j/hcr1*-NTD (row 4), YEp-*j/hcr1*-CTD (row 5), YEp-*j/hcr1*-NTA1 (row 6), and YEp-*j/hcr1*-NTD-NTA1 (row 7), respectively, were spotted in four serial 10-fold dilutions on SD (left) or SD containing 30 mM 3-AT (right) and then incubated at 30 °C for 2 and 3 days, respectively. (b) *j/hcr1Δ* prevents full derepression of *GCN4-lacZ* expression upon starvation. Isogenic H416 (*GCN2 j/HCR1*) and H428 were transformed with p180, grown in minimal media for 6 h, and β -galactosidase activities were measured in WCEs and expressed in nanomoles of *o*-nitrophenyl-*b*-D-galactopyranoside hydrolyzed per minute per milligram of protein. To induce *GCN4-lacZ* expression, we treated transformants grown in minimal media for 2 h with 10 mM 3-AT for 6 h. The table gives means and standard deviations obtained from at least six independent measurements with three independent transformants, and activity in *j/hcr1Δ* relative to wt, respectively. (c and d) Deletion of *j/hcr1Δ* or its NTD only dramatically increases leaky scanning. H428 transformants bearing YEp-*j/HCR1*, YEplac181, YEp-*j/hcr1*-CTD, YEp-*j/hcr1*-NTD, and YEp-*j/hcr1*-NTA1, respectively, were transformed with pM226 (c) and plig102-3 (d), respectively, and analyzed as in (b), except that they were not treated with 3-AT. (e) Overexpression of eIF1A partially suppresses the leaky scanning defect of *j/hcr1Δ*. Strains H416 and H428 transformed with the empty vector and YEpTIF11 (eIF1A), respectively, were transformed with plig102-3 and analyzed as in (d). (f) Overexpression of eIF1A partially suppresses the *Slg⁻* and *Gcn⁻* phenotypes of *j/hcr1Δ*. Strains H428 and H416 transformed with the empty vector and YEpTIF11, respectively, were spotted in four serial 10-fold dilutions on SD or SD + 30 mM 3-AT and incubated at 30 °C for 2 or 4 days.

RRM₁₇₀₋₂₇₄ in complex with hElF3j₃₅₋₆₉ by high-resolution NMR spectroscopy. Stereo views of the 10 lowest-energy structures (Supplementary Fig. 1) and structural statistics (Table 1) demonstrate a

well-defined complex structure with low pairwise rmsd values of 1.19 ± 0.4 Å for heavy atoms corresponding to residues 180–266 and 45–55 of hElF3b-RRM and hElF3j, respectively. The structure of

Table 1. Structural statistics of the heIF3b-RRM_{170–275}–heIF3j_{35–69} complex

<i>Restraints used for structure calculations</i>	
Total NOE distance restraints	1853
Short range (intraresidue)	966
Medium range ($1 < i-j < 5$)	289
Long range ($ i-j \geq 5$)	566
Intermolecular	32
Dihedral-angle restraints (ϕ and ψ)	113
<i>Structural statistics</i>	
Ramachandran plot ^a (%)	
Residues in the most favored regions	71.4
Residues in additionally allowed regions	27.0
Residues in generously allowed regions	1.3
Residues in disallowed regions	0.4
<i>rmsd of atomic coordinates (Å)</i>	
heIF3b-RRM _{184–268} –heIF3j _{45–55} complex	
Backbone atoms	0.726
All heavy atoms	1.192

The 10 conformers with the lowest energies were selected for statistical analysis. Because of the absence of medium-range, long-range, and intermolecular NOEs involving residues 35–44 and 58–69 of heIF3j_{35–69}, these residues were not included in the calculations.

^a Based on PROCHECK-NMR analysis.

heIF3b-RRM in the complex presents a typical RRM fold consisting of two perpendicular α helices packed against a four-stranded anti-parallel β -sheet (Fig. 4a and b).^{33,34} The heIF3j N-terminal peptide is unstructured in free form (data not shown) and binds heIF3b-RRM in an extended conformation on the surface opposite to the β -sheet area of heIF3b-RRM (Fig. 4b). The heIF3j binding surface on heIF3b-RRM comprises helix α 1 and L5. Eleven of 35 residues (Asp45–Asp55) of the negatively charged heIF3j_{35–69} peptide, which are part of its NTA, directly contact heIF3b-RRM (Fig. 4c). The total buried surface area of the protein–protein interface is 1128.4 Å² (501.6 Å² on the heIF3b-RRM peptide and 626.8 Å² on the heIF3j peptide). The heIF3b-RRM interaction surface is characterized by positively charged residues from helix α 1 (Arg199, Lys202, Lys209, and Lys213) and L5 (Lys254) that complement and position the negatively charged heIF3j_{35–69} peptide (Fig. 4c). These interactions are illustrated by intermolecular nuclear Overhauser enhancements (NOEs) that bring Lys254–H ϵ into close contact with Asp54–H α , Lys254–H γ into close contact with Asp54–H β , Lys202–H ϵ into close contact with Val48–H γ , and Lys209–H β into close contact with Asp45–H α , respectively (Supplementary Fig. 2b). At the center of the NTA resides the highly conserved Trp52, which establishes a series of close contacts with heIF3b-RRM (Fig. 4c). The indole ring of Trp52 fills a hydrophobic pocket formed by residues from helix α 1 (Leu203, Val206, and Ile210) and L5 (Tyr253, Leu255, and Phe261) (Fig. 4d). Intermolecular NOEs involving Trp52 ring atoms, such as H δ ¹ and H ϵ ², with Ile210 and Ile207, as well as with Tyr253 and Leu255, represent key contacts for defining the hydrophobic pocket around Trp52 (Supplementary

Fig. 2b). Binding of heIF3j unfolds the β -hairpin in L5 and induces a rearrangement of helix α 1 and L5, as compared to the unbound heIF3b-RRM (Fig. 4e). This creates a more compact heIF3b-RRM conformation illustrated by a closer contact between Ile210 and Tyr253, which deepens the binding pocket filled by Trp52 of heIF3j.

Mutational analysis of the heIF3b-RRM–heIF3j-NTA interaction

To assess the relative contribution of key residues to heIF3b-RRM–heIF3j complex formation, we mutated several important interface residues. Binding of four heIF3j mutants (heIF3j-N51A, heIF3j-N51A-W52A, heIF3j-W52A, and heIF3j-D50K-D53K-D57K) to heIF3b-RRM was examined using isothermal titration calorimetry (ITC). The heIF3j mutants displayed significantly lower affinities than wt heIF3j ($K_d = 20.3 \pm 0.4$ μ M). In this assay, we were unable to detect any heIF3b-RRM binding to heIF3j-W52A, heIF3j-N51A-W52A, and heIF3j-D50K-D53K-D57K, indicating K_d values larger than 10 mM, whereas heIF3j-N51A bound with a lower K_d of 55 ± 0.3 μ M (Fig. 5a). These results agree with our complex structure showing that heIF3j-Trp52 makes crucial hydrophobic contributions to heIF3b-RRM binding and that surrounding negatively charged heIF3j-NTA residues further stabilize complex formation (Fig. 4c).

We also performed histidine pull-down assays using three heIF3b-RRM mutants (heIF3b-RRM-F261A, heIF3b-RRM-I210A, and heIF3b-RRM-Y253A) to assess the contributions of hydrophobic heIF3b-RRM residues to heIF3j binding. All three heIF3b-RRM mutants displayed significantly reduced binding compared to wt heIF3b-RRM, validating the role of the heIF3b-RRM hydrophobic pocket in heIF3j recognition (Fig. 5b and c). Interestingly, hydrophobic amino acid residues in positions Leu203, Val206, Ile210, Tyr253, and Phe261 are highly conserved among eIF3b-RRMs from other species, indicating that the heIF3b-RRM–heIF3j recognition mode is preserved in other organisms (Supplementary Fig. 3).

Molecular determinants of eIF3j–eIF3b-RRM interaction are conserved throughout evolution

To investigate whether the critical determinants of the eIF3b–eIF3j interaction in yeast are similar in nature to those in humans, we first fused both halves of j/HCR1 in j/hcr1-NTD (residues 1–135) and j/hcr1-CTD (residues 136–265) (Fig. 6b) with the GST moiety and showed that the NTD, but not the CTD, of j/HCR1 specifically interacts with the ³⁵S-labeled fragment comprising b/PRT1-RRM (Fig. 6c, lane 4 versus lane 5). We then substituted the Trp37 residue corresponding to the key Trp52 of heIF3j and several surrounding acidic residues from its NTA with alanines or amino acids with the opposite charge (Fig. 6b). The resulting j/hcr1-NTA1 mutation completely abolished binding to radiolabeled b/PRT1-RRM (Fig. 6c, lane 6). Similarly, alanine and

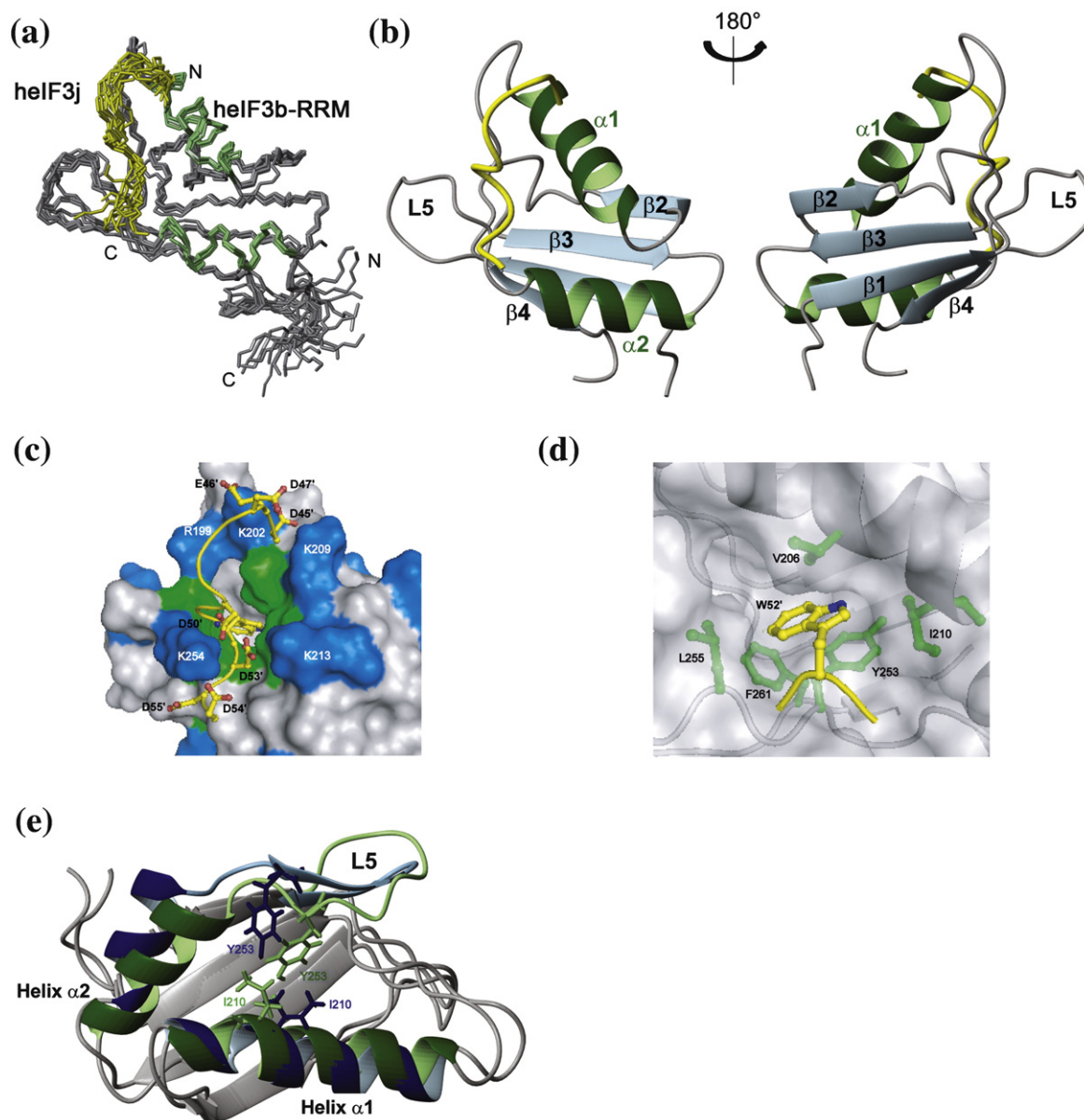


Fig. 4. Structure of the heIF3b-RRM-heIF3j complex. (a) NMR ensemble of the heIF3b-RRM-heIF3j peptide complex. The 10 lowest-energy structures between heIF3b-RRM_{179–274} (gray and green) and heIF3j_{45–55} (yellow) are shown. The structures were fitted using the backbone atoms C', C^α, and N of residues 184–264 of heIF3b-RRM and residues 45–55 of heIF3j. (b) Ribbon model for the lowest-energy conformer of the heIF3b-RRM (gray and green)-heIF3j (yellow) complex. Secondary structure elements of heIF3b-RRM are labeled. (c) Surface representation of contacts between the heIF3j peptide and heIF3b-RRM. Green and blue surfaces indicate hydrophobic and basic (labeled) heIF3b-RRM residues, respectively. heIF3j peptide is shown as a ribbon ball-and-stick representation, and most of its residues are numbered with primed numbers. The lowest-energy structure of heIF3b-RRM bound to the heIF3j peptide is shown. (d) Close-up view of the hydrophobic pocket binding the heIF3j peptide. heIF3b-RRM is displayed as a grayish semitransparent solvent-accessible surface with labeled hydrophobic side chains (green) shown below the surface. These residues form the walls of the hydrophobic pocket in which the aromatic ring of W52' of the heIF3j peptide (yellow) is inserted (residues 51–53 only). (e) Comparison of the NMR structures of free heIF3b-RRM and heIF3j-bound heIF3b-RRM. The two structures are represented as ribbon models, with helices α1 and α2 and L5 shown in green for heIF3j-bound heIF3b-RRM and in blue for free heIF3b-RRM. The side chains of Y253 and I210 are shown in stick representation using the same coloring scheme to highlight closer contacts participating in a more compact conformation of heIF3b-RRM when bound to heIF3j.

opposite charge substitutions of the b/PRT1-RRM residues corresponding to critical residues in helix α1 and L5 of heIF3b in *b/prt1-α1 + L5* (Fig. 6a) eliminated the interaction with GST-j/hcr1 (Fig. 6c, row 3).

To further determine whether disrupting this contact will prevent j/HCR1 association with eIF3

in vivo, we analyzed the formation of the entire eIF3-containing MFC in yeast cells by Ni²⁺ chelation chromatography using His₈-tagged *b/PRT1* as bait. As reported previously,²⁷ a fraction of a/TIF32, j/HCR1, eIF2, eIF5, and eIF1 copurified specifically with wt *b/PRT1*-His, but not with its untagged

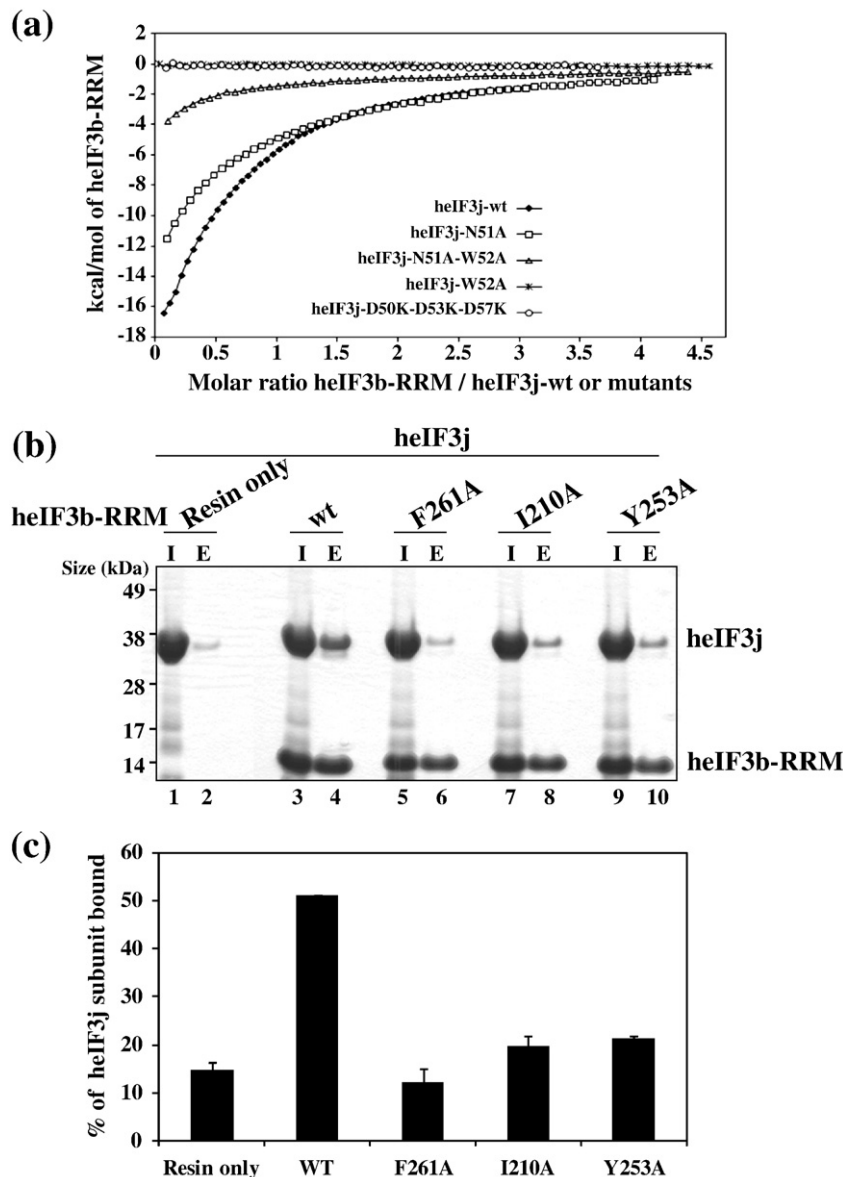


Fig. 5. Mutational analysis of the heIF3b-RRM–heIF3j-NTA interaction. (a) ITC of wt and mutant heIF3j with heIF3b-RRM. The panel shows fitted binding isotherms. Data points were obtained by integration of heat signals plotted against the molar ratio of heIF3b-RRM to wt or mutant heIF3j in the reaction cell. The continuous line represents a calculated curve using the best-fit parameters obtained by a nonlinear least-squares fit. The heIF3j construct used for each experiment is indicated in the panel. (b) Histidine pull-down assays using His₆-tagged wt or mutant heIF3b-RRM and untagged heIF3j. SDS-PAGE analysis of input (I) and eluted (E) fractions from the pull-down experiments, where the untagged heIF3j subunit was used with wt or mutant (F261A, I210A, and Y253A) heIF3b-RRM, as well as resin only as a control. (c) Quantification of the heIF3j fraction bound to heIF3b-RRM by analyzing the band intensity of the eluted fraction compared to the same band in the input fraction. Error bars represent the standard deviation between two individual experiments.

version (Fig. 7a, lanes 5–8 *versus* lanes 1–4). In sharp contrast, the *b/prt1-α1+L5* mutation (LFSK63-66AAAE_HRLF114-117AALA; Fig. 6a) specifically eliminated the association of only j/HCR1 (Fig. 7a, lanes 9–12). Similarly, the *j/hcr1-NTA1* mutation (V33A_Q35A_W37A_D38R_EEEE40-43RRRR; Fig. 6b) diminished the binding of j/HCR1 to the purified b/PRT1-His complex (Fig. 7b, lanes 9–12 *versus* lanes 5–8).

Finally, disrupting j/HCR1-NTA–b/PRT1-RRM interaction by *j/hcr1-NTA1* and *b/prt1-α1+L5* mutations, respectively, in living cells resulted in the

Slg[−] phenotype (Fig. 1e, row 5; Fig. 7c, row 2). No growth phenotype was observed with less extensive mutations in the HCR1-NTA1 motif or when helix α1 and L5 of PRT1 were mutated separately, arguing against the general refolding problems of these two motifs (data not shown).

***b/prt1-α1+L5* mutation strongly affects the 40S association of eIF3**

As mentioned above, the *b/prt1-rnp1* mutation substituting for the conserved residues of the RNP1

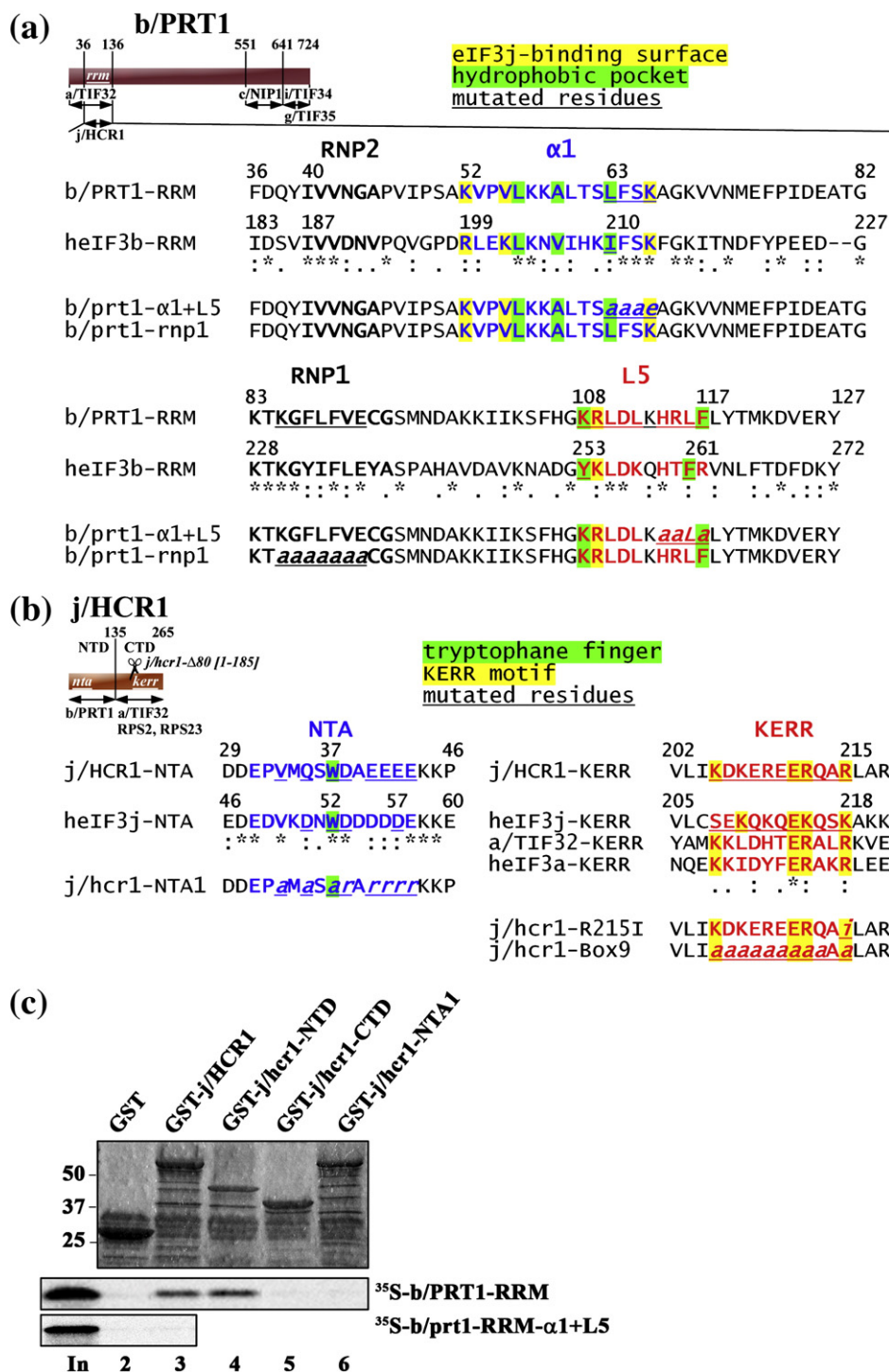


Fig. 6. Molecular determinants of the eIF3j-eIF3b-RRM interaction are evolutionary conserved. (a) Schematic of b/PRT1 showing the position of RRM (*rrm*). Arrows delimit minimal binding domains for the indicated proteins. The positions of RNPs (black), helix $\alpha 1$ (blue), and L5 (red) are indicated above the sequences aligned using the GCG Analysis Program. Residues corresponding to the heIF3j binding surface are highlighted in yellow; residues forming the hydrophobic pocket are highlighted in green. Underlined are b/PRT1 residues that were subjected to site-directed mutagenesis in this study or in previous studies.¹² (b) Same as in (a), except that the schematic of j/HCR1 is shown with locations of the NTA (*nta*), the C-terminal KERR motif (*kerr*), and the C-terminal truncation ($\Delta 80$). Sequences surrounding the NTA and KERR motifs of yeast and heIF3j or human eIF3a, respectively, are indicated. Underlined are j/HCR1 residues that were subjected to site-directed mutagenesis in this study or in previous studies.²⁵ The human Trp52 and the corresponding yeast Trp37 are highlighted in green; the key residues of the KERR motif are highlighted in yellow. (c) Full-length j/HCR1 (lane 3), its N-terminal domain (lane 4) or C-terminal domain (lane 5), the NTA1 mutant (lane 6) fused to GST, and GST alone (lane 2) were tested for binding to ³⁵S-labeled wt b/PRT1-RRM [1-136] and b/PRT1-RRM- $\alpha 1$ +L5; 10% of input amounts added to each reaction are shown in lane 1 (In).

motif forming the $\beta 3$ strand of the four-stranded anti-parallel β -sheet with a stretch of alanines (Fig. 6a) eliminated j/HCR1 from the MFC¹² and severely affected the binding of the mutant form of eIF3 with the 40S subunit.¹² While this mutation occurs on the side opposite to that directly engaged in interacting with j/HCR1, based on our NMR structure,²⁰ it changes two amino acids in heIF3b-RRM (I233 and L235) and presumably also in b/PRT1-RRM at equivalent positions (L88 and V90), contributing to the hydrophobic core of the RRM

fold. It is therefore conceivable that these substitutions interfere with proper folding; thus, the effects of *b/prt1-rnp1* cannot be directly related to the specific loss of contacts that the RRM of b/PRT1 makes. This assumption gains support from our observation that the Slg⁻ phenotype of *b/prt1-rnp1*, but not of *b/prt1- $\alpha 1$ +L5*, can be partially suppressed by high-copy j/HCR1 through mass action (Fig. 2f; data not shown). It is understandable that the elevated protein mass can drive the establishment of only that interaction, whose key determinants

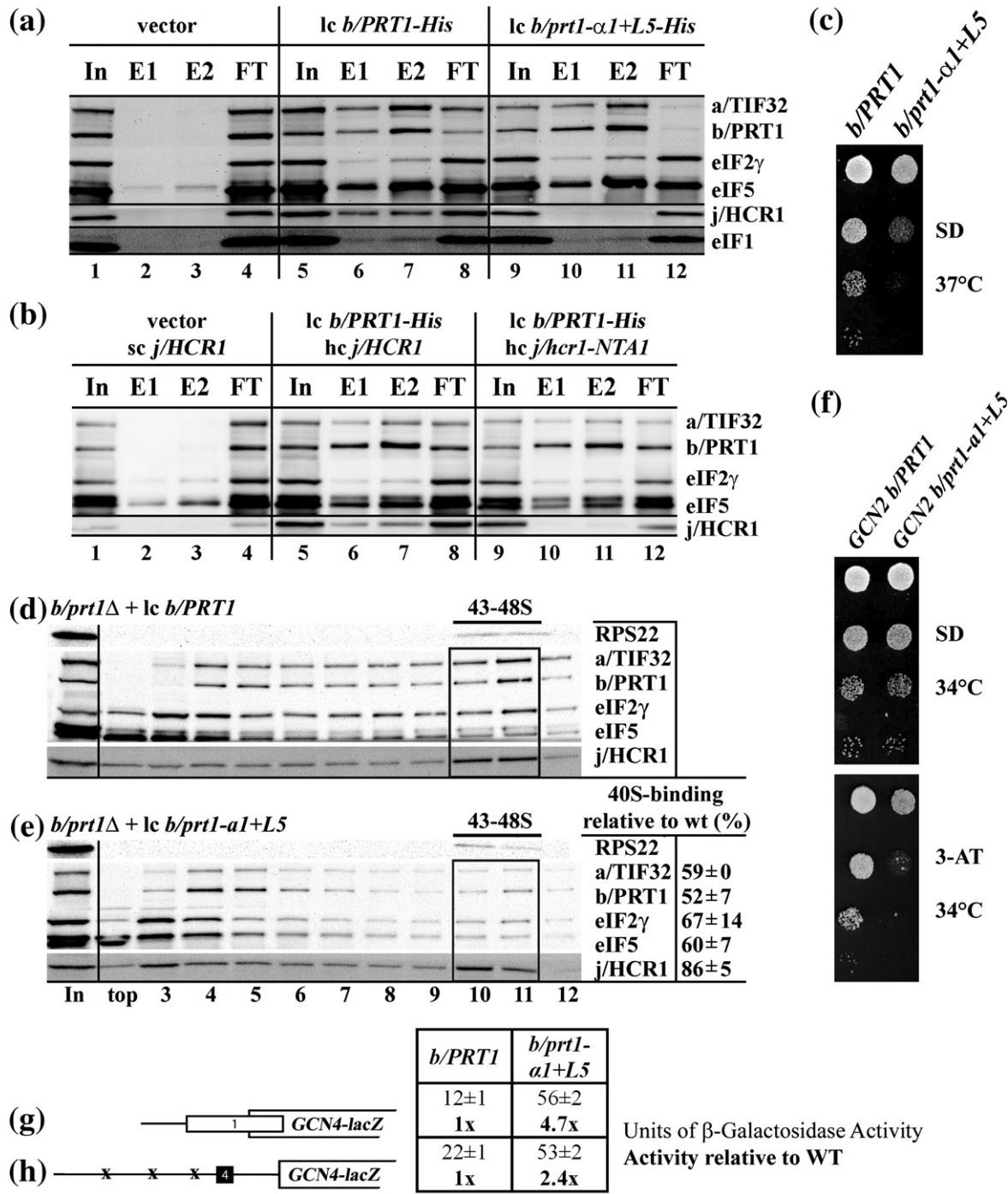


Fig. 7 (legend on next page)

remain preserved in spite of potential destabilization of the protein fold.

To examine whether the *b/prt1- α 1+L5* mutation specifically disrupting direct j/HCR1–b/PRT1-RRM contact also affects the 40S association of mutant eIF3, we measured the binding of selected eIF3 subunits and other MFC components to 40S subunits by formaldehyde cross-linking. We observed a relative ~45% decrease in the amounts of selected eIF3 subunits associated with 40S subunits in whole-cell extracts (WCEs) obtained from *b/prt1- α 1+L5* cells compared to wt control (Fig. 7d and e, fractions 10 and 11). Similar reductions were also observed for eIF5 (~40%) and eIF2 (~35%). In keeping with our previous finding with *b/prt1-rnp1*,¹² amounts of the 40S-associated j/HCR1 were reduced only marginally (~15%). Since, under the conditions of our experiments, the data suggest that j/HCR1 does not play a key role in eIF3 association with the 40S subunit, this dramatic defect cannot be fully attributable to the loss of the j/HCR1–b/PRT1-RRM interaction, implying that helix α 1 and L5 residues are most probably directly involved in bridging the 40S–eIF3 contact in yeast. Nevertheless, our observations that the *NTA1* mutation, which did not affect the 40S–eIF3 interaction (data not shown), failed to suppress the Slg[–] phenotype of *b/prt1-rnp1* (Fig. 2f, last row) and that its own Slg[–] phenotype was found to be partially suppressible by a plasmid overexpressing all three eIF2 subunits and tRNA^{Met} (hc TC) (Fig. 2e, last two rows) seem to indicate that it does compromise the mild stimulatory effect of j/HCR1 on 40S binding by eIF3.

j/HCR1–b/PRT1-RRM interaction prevents leaky scanning over the AUG start codon

Our finding that the deletion of the NTD of j/HCR1 produced severe leaky scanning (Fig. 3c and

d) and the fact that a modest leaky scanning defect was also observed with *b/prt1-rnp1*¹² provoked us to test whether disrupting the specific contact between j/HCR1 and b/PRT1-RRM will affect the level of leaky scanning in mutant cells. Indeed, *j/hcr1-NTA1* and *j/hcr1-NTD-NTA1* mutants displayed 3-AT sensitivity (Fig. 3a, last two rows) and greatly increased leaky scanning over uORF4 by ~4-fold (Fig. 3d, column 5). Similarly, the *b/prt1- α 1+L5* mutant showed a reduced growth rate in the presence of 3-AT even at 34 °C (Fig. 7f) and also significantly increased leaky scanning over elongated uORF1 by ~4.7-fold (Fig. 7g) and over uORF4 by ~2.4-fold (Fig. 7h). Hence, these data strongly suggest that the evolutionary conserved j/HCR1–NTA–b/PRT1-RRM interaction ensures tight control over the stringent selection of the proper AUG start codon.

Discussion

NMR solution structure of the heIF3b-RRM–heIF3j-NTA interaction

eIF3 plays critical roles in virtually all stages of translation initiation, during reinitiation, in posttermination ribosomal recycling, and in the nonsense-mediated decay pathway.^{8,9,35,36} In understanding how the numerous functions of eIF3 are encoded in its conserved subunits and their interactions, high-resolution structural studies of protein–protein interactions of eIF3 subunits are imminent. Using NMR spectroscopy, we revealed the first structure of an interaction among eIF3 subunits (between heIF3b-RRM and heIF3j-NTA) (Fig. 4) and showed that its disruption in yeast eliminated j/HCR1 association with MFC *in vivo* (Fig. 7). This interaction is driven by a conserved charge

Fig. 7. Destroying the hydrophobic pocket of the RRM of b/PRT1 prevents j/HCR1 association with eIF3 *in vivo*, reduces eIF3 binding to 40S subunits, and increases leaky scanning. (a and b) The NTA of j/HCR1 and helix α 1 and L5 of b/PRT1-RRM are critically required for j/HCR1 association with MFC *in vivo*. (a) WCEs were prepared from H425 (*b/prt1 Δ*) bearing untagged b/PRT1 (lanes 1–4), and H425 transformants with pRS-b/PRT1-His (lanes 5–8) and pRS-b/PRT1-L5+ α 1-His (lanes 9–12) from which the untagged b/PRT1 was evicted on SD plates containing 5-fluoroorotic acid, respectively, were incubated with Ni²⁺ silica resin, and the bound proteins were eluted and subjected to Western blot analysis, with antibodies indicated on the right-hand side of individual strips. Lanes 1, 5, and 9 contained 5% of input WCEs (In); lanes 2, 6, and 10 contained 30% of fractions eluted from the resin (E1); lanes 3, 7, and 11 contained 60% of the same fractions (E2); and lanes 4, 8, and 12 contained 5% of flow-through (FT). (b) WCEs prepared from double transformants of H428 (*j/hcr1 Δ*) bearing pRS315 and YCp-j/HCR1-DS-U (lanes 1–4), pRS-b/PRT1-His and YEp-j/HCR1-DS-U (lanes 5–8), or pRS-b/PRT1-His and YEp-j/hcr1-NTA1-U (lanes 9–12), respectively, were analyzed as in (a). (c–e) Mutating the hydrophobic pocket of the RRM of b/PRT1 results in the Slg[–] phenotype and strongly affects the 40S association of eIF3. (c) H425 transformants as in (a) were spotted in four serial 10-fold dilutions on SD medium and incubated at 37 °C for 2 days. (d and e) H425 transformants as in (a) were grown in SD medium at 37 °C to an OD₆₀₀ of ~1.5 and analyzed as in Fig. 3a–d, except that the resedimentation protocol was not applied. Mean proportions of the total proteins found in fractions 10 and 11 were calculated using NIH ImageJ from two independent experiments. The resulting values obtained with the indicated eIFs with the wt strain were set to 100%, and those obtained with the mutant strain were expressed as percentages of wt (SD given). (f–h) The *b/prt1- α 1+L5* mutation impairs derepression of GCN4 translation during starvation as a result of leaky scanning. (f) *b/prt1- α 1+L5* imparts the Gcn[–] phenotype. YAH06 (*GCN2 b/prt1 Δ*) transformants carrying pRS-b/PRT1-His and pRS-b/prt1-L5+ α 1-His, respectively, were spotted in four serial 10-fold dilutions on SD (top) or SD containing 30 mM 3-AT (bottom) and then incubated at 34 °C for 2 and 3 days, respectively. (g and h) *b/prt1- α 1+L5* strongly increases leaky scanning. YAH06 transformants as in (f) were transformed with pM226 (g) and plig102-3 (h), respectively, and analyzed as in Fig. 5c and d.

complementarity between the subunits and an evolutionary conserved hydrophobic pocket on the backside of heIF3b-RRM, which accommodates the strictly conserved Trp residue in heIF3j-NTD (Supplementary Fig. 3). This recognition mode is also employed by the UHM family (U2AF homology motif) of noncanonical RRM, which mediate protein-protein interactions through a conserved Arg-X-Phe motif in L5 and a negatively charged extended helix α 1. UHM-ligand complexes share the crucial role of a conserved Trp residue from the ligand buried in a hydrophobic RRM pocket at the center of the protein interface, as in the case of the heIF3b-RRM-heIF3j complex,^{37–39} suggesting a general mode of protein recognition by these noncanonical RRM (Fig. 4).

eIF3j contributes to the delicate process of setting the reading frame for decoding, in cooperation with its conserved binding partner eIF3b-RRM and with eIF1A

In this study, we presented two unexpected findings on the role(s) of the j/HCR1 subunit of eIF3 in translation: (i) its NTD is sufficient to fulfill all functions of j/HCR1 needed to support the wt growth of yeast cells (Fig. 1e); and (ii) j/HCR1 is required for maintaining proper control over the AUG start codon selection, in cooperation with its binding partner b/PRT1 and with eIF1A (Fig. 3), implying that it most likely stays ribosome bound beyond mRNA recruitment, at least to the point of AUG recognition.

Consistent with the placement of heIF3j-CTD in the mRNA entry channel and ribosomal A site,¹⁵ our *in vitro* binding assays revealed specific interactions between the CTD of j/HCR1 and RPS2 and RPS23, depending on its KERR motif (Fig. 1b and c). RPS23 is situated on the interface side under the A site, whereas RPS2 lies on the solvent side at the entry pore of the mRNA channel (Fig. 1d).¹⁶ Placing the CTD of j/HCR1 into the mRNA entry channel suggests that the NTD of j/HCR1 most probably resides at the entry pore on the 40S solvent side, where the main body of eIF3 is thought to reside and thus where it could interact with the RRM of b/PRT1 (Fig. 1a).^{14,18} (The RRM of b/PRT1 interacts with the C-terminal part of the a/TIF32 subunit,¹⁰ which is also believed to occur near the entry pore of the mRNA binding track based on its previously reported interactions with helices h16–h18 and RPS0A.^{8,14})

Given its specific location and its observed negative cooperativity with mRNA in 40S binding,¹⁵ heIF3j was predicted to regulate access of the mRNA-binding cleft and to influence mRNA–40S subunit association during scanning and AUG recognition.¹⁵ Our results showing that deletion of j/HCR1 or of its NTD produces a severe leaky scanning defect (Fig. 3c and d) are in perfect agreement with this prediction and suggest that eIF3j may contribute to the stabilization of the

properly formed preinitiation complexes at the start codon. A similar role in pausing scanning upon establishment of a correct initiation codon–anticodon base-pairing was proposed for eIF1A.³⁰ Interestingly, heIF3j showed negative cooperativity in 40S binding also with eIF1A,¹⁵ and we indeed observed that the leaky scanning phenotype was partially (by ~50%) suppressed by overexpressing eIF1A (Fig. 3e). Furthermore, we found that destroying the specific contact between j/HCR1-NTA and b/eIF3b-RRM by NTA1 and α 1+L5 mutations, respectively, also greatly increased leaky scanning phenotype, although not to the same extent as the deletion of the entire NTD (Figs. 3 and 7). Hence, it is conceivable that other regions of the NTD of j/HCR1 are further required for wt function. Given the fact that the b/PRT1 RRM but not j/HCR1 plays a critical role in stable eIF3 association with the 40S subunit (see the text below), these results strongly suggest that the major role of the evolutionary conserved interaction between eIF3j and eIF3b is to prevent skipping over the proper AUG start codon during scanning. Based on these observations, we propose the following model (Fig. 8).

Both terminal domains of yeast j/HCR1 make independent but synergistic interactions with the region on the 40S subunit, including the 40S mRNA entry channel, to at least partially block mRNA recruitment (Fig. 8a). It was shown that negative cooperativity between heIF3j and mRNA is neutralized upon TC recruitment to the P site, even though heIF3j remains in the mRNA-binding cleft.¹⁵ Hence, we further propose that the recruitment of TC with other eIFs, including eIF3, may act together to clear the entry pore for mRNA recruitment, perhaps partially via establishment of j/HCR1-NTA–b/PRT1-RRM interaction (Fig. 8b). Upon commencement of scanning, eIF3j/HCR1, in cooperation with eIF3b/PRT1-RRM, most probably makes an indirect functional contact with eIF1A that could influence the conformation and activity of eIF1A in helping to decode the initiation codon in a way that would prevent leaky scanning, possibly by prompt switching to the scanning-arrested conformation when the start codon has entered the P site (Fig. 8c).

j/HCR1 was previously shown to stimulate 40S binding by eIF3 *in vivo*¹² and by its human orthologue *in vitro*.^{7,22,28} Our *in vivo* formaldehyde cross-linking experiments (Fig. 2), combined with unpublished *in vitro* 40S–eIF3±j binding data from J. Lorsch's laboratory (J. Lorsch, personal communication, 2009), however suggest that this stimulatory activity of j/HCR1 might not be as strong as initially thought. With respect to this, the strong requirement of heIF3j for bringing purified eIF3 to the 40S subunit seems to indicate that yeast and human j subunits differ in the extent of this stimulation. Nevertheless, given the fact that the heIF3j requirement for 40S binding by eIF3 was suppressed by the TC, eIF1, eIF1A, or single-stranded RNA or DNA cofactors,^{7,28} the physiological significance of these *in vitro* observations with heIF3j will require careful examination in living mammalian cells.

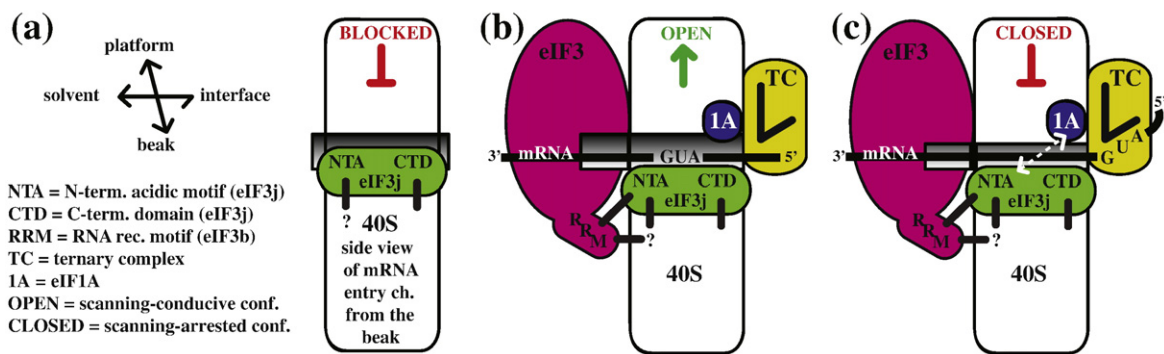


Fig. 8. eIF3j/HCR1 cooperates with eIF3b/PRT1 and eIF1A to ensure stringent selection of the AUG start codon. (a) In the absence of eIFs, eIF3j/HCR1 occupies the mRNA entry channel to at least partially block mRNA recruitment. (b) Recruitment of TC and eIF3 that interacts with the NTA of eIF3j/HCR1 via the RRM of eIF3b/PRT1 clears the mRNA entry channel, so that the ribosome can adopt the open/scanning-conductive conformation for mRNA recruitment. (c) Upon AUG recognition, eIF3j/HCR1, in cooperation with eIF3b/PRT1-RRM, functionally interacts with eIF1A to stimulate prompt switching to the closed/scanning-arrested conformation. Black thick lines represent direct interactions; the dotted line with arrowheads indicates functional interaction between eIF3j/HCR1 and eIF1A.

Unlike the *j/hcr1-NTA1* mutation, mutation of the conserved hydrophobic pocket residues in *b/prt1-α1 + L5* dramatically reduced 40S occupancy by eIF3 and its associated eIFs *in vivo* (Fig. 7e). These findings strongly indicate that this activity of the b/PRT1-RRM region comprising the hydrophobic pocket is independent of its contact with the NTA of j/HCR1. Hence, we propose that the RRM features helix α1 and L5, in addition to preventing leaky scanning by interacting with j/HCR1, most likely also form an important intermolecular bridge between eIF3 and the 40S subunit (Fig. 8b) such as that created by the NTD of a/TIF32 and RPS0a.^{8,14}

Finally, it is noteworthy that the expression of *j/hcr1-NTD* or CTD alone suppressed the 40S biogenesis defect of *j/hcr1Δ* cells²⁷ only partially (S.W. and L.V., unpublished observations), implying that the full-length j/HCR1 is needed for optimal function. Since *j/hcr1-NTD* fully supports wt growth, we find it highly unlikely for the 40S biogenesis defect to significantly contribute to *j/hcr1Δ* growth defects.

Materials and Methods

Construction of yeast strains and plasmids

To create SY73, we introduced H428 with YEp-j/hcr1-NTA1, and we selected the resulting transformants on media lacking leucine.

YAH06 was generated by a genetic cross of H426 (Table 2; same as H425 only MAT'alpha') and H428 (Table 2).¹² After tetrad dissection, spores with the slow-growth phenotype suppressible by *j/HCR1*, resistant to 3-AT, unable to grow on media containing 5-fluoroorotic acid, and autotrophic for tryptophan were selected.

A list of all PCR primers named below can be found in [Supplementary Table 1](#):

pGEX-j/hcr1-NTD was made by inserting the BamHI-Sall-digested PCR product obtained with primers AD GST-HCR1 and AH-GST-HCR1-NTD-R, using the

template pGEX-j/HCR1, into BamHI-Sall-digested pGEX-5X-3.

pGEX-j/hcr1-CTD was made by inserting the BamHI-Sall-digested PCR product obtained with primers AH-GST-HCR1-CTD and AD GST-HCR1-R, using the template pGEX-j/HCR1, into BamHI-Sall-digested pGEX-5X-3.

pGEX-j/hcr1-NTA1 was made by inserting the BamHI-Sall-digested PCR product obtained with primers AD GST-HCR1 and AD GST-HCR1-R, using the template YEp-j/hcr1-NTA1 (see the text below), into BamHI-Sall-digested pGEX-5X-3.

pT7-b/prt1-rrm-α1+L5 was made by inserting the NdeI-HindIII-digested PCR product obtained with primers LVPNDEI-724 and LVPC136-724, using the template pRS-b/prt1-L5+α1-His (see the text below), into NdeI-HindIII-digested pT7-7.⁴⁰

pGEX-j/hcr1-BOX9 was made by inserting the BamHI-Sall-digested PCR product obtained with primers AD GST-HCR1 and AD GST-HCR1-R, using the template YEp-j/hcr1-BOX9 (see the text below), into BamHI-Sall-digested pGEX-5X-3.

pGEX-j/hcr1-Δ80 was made by inserting the BamHI-NcoI-digested PCR product obtained with primers AD GST-HCR1 and HCR1-80-NcoI-R, using the template YEp-j/HCR1-DS, into BamHI-NcoI-digested pGEX-5X-3.

pGEX-RPS2 was made by inserting the BamHI-Sall-digested PCR product obtained with primers RPS2-f

Table 2. Yeast strains used in this study

Strain	Genotype	Source or reference
H416 ^a	<i>MATa leu2-3,112 ura3-52</i>	Nielsen <i>et al.</i> ¹²
H417 ^a	<i>MATa leu2-3,112 ura3-52 trp1Δ</i>	Nielsen <i>et al.</i> ¹¹
H425 ^a	<i>MATa leu2-3,112 ura3-52 trp1Δ</i> <i>b/prt1::hisG gcn2::hisG</i> (<i>lc b/PRT1 URA3</i>)	Nielsen <i>et al.</i> ¹²
H428 ^a	<i>MATa leu2-3, 112 ura3-52 j/hcr1Δ</i>	Nielsen <i>et al.</i> ¹²
SY73 ^a	<i>MATa leu2-3, 112 ura3-52 j/hcr1Δ</i> (<i>hc j/hcr1-NTA1 LEU2</i>)	This study
YAH06	<i>MATa leu2-3,112 ura3-52 trp1Δ</i> <i>b/prt1::hisG GCN2 (lc b/PRT1 URA3)</i>	This study
H3674 ^a	<i>MATa leu2-3, 112 ura3-52 b/prt1-rmp1</i>	Nielsen <i>et al.</i> ¹²

^a Isogenic strains.

and RPS2-r, using the template pGBKT7-RPS2,¹⁴ into BamHI-SalI-digested pGEX-5x-3.

pGBK-T7-RPS23 was made by inserting the BamHI-PstI digested PCR product obtained with primers RPS23-f and RPS23-r, using the template pGBKRPS23,¹⁴ into BamHI-PstI cleaved pGBKT7 (Novagen).

To construct pRS-b/PRT1-HisXS, we used a pair of primers (AH-PRT1-BamHI and AH-PRT1-NotI-R), with pRSPRT1-His-LEU¹² as template. The PCR product thus obtained was digested with BamHI-NotI and inserted into BamHI-NotI-cleaved pRSPRT1-His-LEU. This subcloning step was performed to remove the second XbaI and SpeI sites immediately following the stop codon of b/PRT1 to facilitate subcloning of the RRM mutants.

pRS-b/prt1-L5+ α 1-His was constructed in two steps. First, two pairs of primers (AH-PRT1-ApaI and LV-RRM-AALA-R, and LV-RRM-AALA-R and AH-PRT1-XbaI-R) were used, with pRS-b/PRT1-HisXS as template. The PCR products thus obtained were used in a 1:1 ratio as templates for a third PCR amplification with primers AH-PRT1-ApaI and AH-PRT1-XbaI-R. The resulting PCR product was digested with ApaI-XbaI and inserted into ApaI-XbaI-cleaved pRS-b/PRT1-HisXS, producing pRS-b/prt1-AALA-His. In the second step, pRS-b/prt1-AALA-His was used as template for PCR with two pairs of primers: AH-PRT1-ApaI and AH-PRT1-A1B-R, and AH-PRT1-A1B and AH-PRT1-XbaI-R. The PCR products thus obtained were used in a 1:1 ratio as templates for a third PCR amplification with primers AH-PRT1-ApaI and AH-PRT1-XbaI-R. The resulting PCR product was digested with ApaI-XbaI and inserted into ApaI-XbaI-cleaved pRS-b/PRT1-HisXS.

YEp-j/HCR1-DS was constructed using the QuikChange® Multi Site-Directed Mutagenesis Kit (Stratagene) in accordance with the vendor's instructions. In step 1, PCR was performed with the kit-provided enzyme blend using primers DS HCR1-BHI and DS HCR1-NcoI, and YEpHCR1²⁶ as template. This subcloning step was performed to introduce the BamHI site immediately preceding the AUG start codon and the NcoI sites immediately following the stop codon of j/HCR1 to facilitate subcloning of the j/HCR1 mutants.

YCp-j/HCR1-DS-U was constructed by inserting the 1289-bp HindIII-SacI fragment from YEp-j/HCR1-DS into YCpLVHCR1-U,²⁶ digested with HindIII-SacI.

YEp-j/HCR1-DS-U was constructed by inserting the 1289-bp HindIII-SacI fragment from YEp-j/HCR1-DS into YEplac195,⁴¹ digested with HindIII-SacI.

YEp-j/hcr1-BOX9 was generated by fusion PCR. The following pairs of primers were used for separate PCR amplifications, using YEp-j/HCR1-DS as template: (1) DS HCR1-BHI and AH-HCR1-BOX+9-R; and (2) AH-HCR1-BOX+9 and AH-HCR1-NcoI-R. The PCR products thus obtained were used in a 1:1 ratio as templates for a third PCR amplification using primers DS HCR1-BHI and AH-HCR1-NcoI-R. The resulting PCR product was digested with BamHI and NcoI and ligated with BamHI-NcoI-cleaved YEp-j/HCR1-DS (replacing wt j/HCR1 with j/hcr1-BOX9).

YEp-j/hcr1-NTA1 was generated by fusion PCR. The following pairs of primers were used for separate PCR amplifications, using YEp-j/HCR1-DS as template: (1) DS HCR1-BHI and HCR1-NTA4-R; and (2) SW-HCR1-NTA2+4 and AH-HCR1-NcoI-R. The PCR products thus obtained were used in a 1:1 ratio as templates for a third PCR amplification using primers DS HCR1-BHI and AH-HCR1-NcoI-R. The resulting PCR product was digested with BamHI and NcoI and ligated with BamHI-

NcoI-cleaved YEp-j/HCR1-DS (replacing wt j/HCR1 with j/hcr1-NTA1).

YEp-j/hcr1-NTA1-U was constructed by inserting the 1289-bp HindIII-SacI fragment from YEp-j/hcr1-NTA1 into YEplac195,⁴¹ digested with HindIII-SacI.

YEp-j/hcr1-NTD was constructed in two steps. First, the 817-bp insert obtained by digestion of pGEX-j/hcr1-NTD with BamHI and NotI was ligated into BamHI-NotI-cleaved pRS303.⁴² The resulting plasmid was then cut with BamHI-SacI, and the insert containing j/hcr1-NTD was used to replace the full-length j/HCR1 in the BamHI-SacI-cut YEp-j/HCR1-DS.

YEp-j/hcr1-CTD was made by inserting the BamHI-NcoI-digested PCR product obtained with primers AH-GST-HCR1-CTD and AH-HCR1-NcoI-R, using YEp-j/HCR1-DS as template, into BamHI-NcoI-cut YEp-j/HCR1-DS (replacing wt j/HCR1 with j/hcr1-CTD).

YEp-j/hcr1-NTD-NTA1 was made by inserting the BamHI-NcoI-digested PCR product obtained with primers DS HCR1-BHI and SW HCR1-NTD-NcoI-R, using YEp-j/hcr1-NTA1 as template, into BamHI-NcoI-cut YEp-j/HCR1-DS (replacing wt j/HCR1 with j/hcr1-NTD-NTA1).

Yeast biochemical methods

GST pull-down experiments with GST fusions and *in-vitro*-synthesized ³⁵S-labeled RPS2, RPS23a, j/hcr1-NTD, j/hcr1-CTD, and b/PRT1-RRM polypeptides (see Table 3 for vector descriptions) were conducted as follows. Individual GST fusion proteins were expressed in *Escherichia coli*, immobilized on glutathione-Sepharose beads, and incubated with 10 μ l of ³⁵S-labeled potential binding partners at 4 °C for 2 h. The beads were washed three times with 1 ml of phosphate-buffered saline, and bound proteins were separated by SDS-PAGE. Gels were first stained with Gelcode Blue Stain Reagent (Pierce) and then subjected to autoradiography. (GST-RPS23 could not be tested due its insolubility in bacterial lysates.) Ni²⁺ chelation chromatography of eIF3 complexes containing His-tagged b/PRT1 from yeast WCEs and Western blot analysis were conducted as described in detail previously.⁴⁸ In short, WCEs were incubated with 4 μ l of 50% Ni²⁺-NTA-silica resin (Qiagen) suspended in 200 μ l of buffer A for 2 h at 4 °C, followed by washing and elution. Fractionation of native preinitiation complexes in WCEs from HCHO cross-linked cells through sucrose gradients, including resedimentation analysis, were carried out in accordance with Valášek *et al.*²⁹

NMR spectroscopy

NMR experiments were performed on Bruker AMX500 or AVANCE800 spectrometers equipped with cryoprobes and on a Bruker DMX600 spectrometer. ¹H, ¹³C, and ¹⁵N chemical shifts assignment was achieved by means of through-bond heteronuclear scalar correlations, with standard pulse sequences recorded on either ¹³C/¹⁵N-labeled hElF3b-RRM complexed with the hElF3j peptide or ¹³C/¹⁵N-labeled hElF3j peptide complexed with hElF3b-RRM in NMR buffer [20 mM deuterated-Tris (pH 7.5) and 100 mM NaCl] containing 10% ²H₂O. Acquisition of NOEs was accomplished using a series of standard three-dimensional (3D) heteronuclear experiments. Intermolecular NOEs between the hElF3b-RRM domain and the hElF3j peptides (long=residues 1–69 of hElF3j, with a deletion of six of seven nonconserved N-terminal alanine residues in accordance with ElAntak *et al.*,²⁰ or short=residues 35–69 of hElF3j) were obtained

Table 3. Plasmids used in this study

Plasmid	Description	Source or reference
pGEX-5X-3	Cloning vector for GST fusions	Smith and Johnson ⁴³
pGEX-j/HCR1	GST-j/hcr1 fusion plasmid from pGEX-5X-3	Valášek <i>et al.</i> ²⁵
pGEX-j/hcr1-NTD	GST-j/hcr1-NTD [1–135] fusion plasmid from pGEX-5X-3	This study
pGEX-j/hcr1-CTD	GST-j/hcr1-CTD [136–265] fusion plasmid from pGEX-5X-3	This study
pGEX-j/hcr1-NTA1	GST-j/hcr1-NTA1 fusion plasmid from pGEX-5X-3	This study
pT7-b/PRT1-RRM (Δ A)	<i>b/PRT1</i> [1–136] ORF cloned under T7 promoter	Valášek <i>et al.</i> ²⁵
pT7-b/prt1-rrm- α 1 + L5	<i>b/PRT1</i> [1–136] ORF containing the α 1 + L5 mutation cloned under T7 promoter	This study
pGEX-j/hcr1-BOX9	GST-j/hcr1-BOX9 fusion plasmid from pGEX-5X-3	This study
pGEX-j/hcr1- Δ 80	GST-j/hcr1- Δ 80 [1–185] fusion plasmid from pGEX-5X-3	This study
pGBK-T7-RPS2	RPS2 ORF cloned into pGBKT7, <i>TRP1</i> (Clontech)	Valášek <i>et al.</i> ¹⁴
pGBK-T7-RPS23	RPS23 ORF (without intron) cloned into pGBKT7, <i>TRP1</i> (Clontech)	This study
pGEX-RPS2	GST-RPS2 fusion plasmid from pGEX-5X-3	This study
pRS-b/PRT1-HisXS	Low-copy wt <i>b/PRT1</i> in <i>LEU2</i> plasmid from pRS315	This study
pRS-b/prt1-L5 + α 1-His	Low-copy <i>b/PRT1</i> containing the α 1 + L5 mutation in <i>LEU2</i> plasmid from pRS315	This study
YEplac181	High-copy cloning vector, <i>LEU2</i>	Gietz and Sugino ⁴¹
YEplac195	High-copy cloning vector, <i>URA3</i>	Gietz and Sugino ⁴¹
YEj/HCR1-DS	High-copy wt <i>j/HCR1</i> coding region flanked by BamHI and NcoI sites, respectively, in <i>LEU2</i> plasmid from YEplac181	This study
YCp-j/HCR1-DS-U	Low-copy wt <i>j/HCR1</i> in <i>URA3</i> plasmid from YCplac33	This study
YEj/HCR1-DS-U	High-copy wt <i>j/HCR1</i> coding region flanked by BamHI and NcoI sites, respectively, in <i>URA3</i> plasmid from YEplac195	This study
YEj/hcr1-NTA1	High-copy <i>j/HCR1</i> containing the <i>NTA1</i> mutation in <i>LEU2</i> plasmid from YEplac181	This study
YEj/hcr1-NTA1-U	High-copy <i>j/HCR1</i> containing the <i>NTA1</i> mutation in <i>URA3</i> plasmid from YEplac195	This study
YEj/hcr1-NTD	High-copy <i>j/hcr1-NTD</i> [1–135] in <i>LEU2</i> plasmid from YEplac181	This study
YEj/hcr1-CTD	High-copy <i>j/hcr1-CTD</i> [136–265] in <i>LEU2</i> plasmid from YEplac181	This study
YEj/hcr1-NTD-NTA1	High-copy <i>j/hcr1-NTD</i> [1–135] containing the <i>NTA1</i> mutation in <i>LEU2</i> plasmid from YEplac181	This study
YEplac24	High-copy cloning vector, <i>URA3</i>	Botstein <i>et al.</i> ⁴⁴
p1780-IMT	High-copy <i>SUI2</i> , <i>SUI3</i> , <i>GCD11</i> , <i>IMT4</i> , and <i>URA3</i> plasmid from YEp24	Asano <i>et al.</i> ⁴⁵
p180 (YCp50-GCN4-lacZ)	Low-copy <i>URA3</i> vector containing wt <i>GCN4</i> leader	Mueller and Hinnebusch ⁴⁶
pM226	Derivative of pM199; ORF of uORF1 extends into the <i>GCN4-lacZ</i> coding region	Grant <i>et al.</i> ³²
plig102-3	Low-copy <i>URA3</i> vector with <i>GCN4</i> leader point mutations containing uORF4 only at its original position in front of the <i>GCN4-lacZ</i> coding region	Grant <i>et al.</i> ³²
pDSO22	High-copy <i>TIF11</i> (eIF1A), <i>URA3</i> plasmid from YEplac195	Olsen <i>et al.</i> ⁴⁷

from two-dimensional (2D) and 3D ¹³C-filtered NOE spectroscopy (NOESY) experiments recorded on ¹³C/¹⁵N-labeled heIF3b-RRM complexed with the long or short heIF3j peptide and on the long or short ¹³C/¹⁵N-labeled heIF3j peptide complexed with heIF3b-RRM in a 100% ²H₂O solution. Comparison of the intermolecular NOE pattern for the short and long heIF3j peptides revealed no significant differences; more importantly, no additional NOEs could be observed with the longer peptide. Therefore, the heIF3b-RRM complex with the shorter heIF3j peptide was chosen for high-resolution structure determination. All NMR samples were prepared in 20 mM deuterated Tris (pH 7.5) and 100 mM NaCl. The concentrations were 0.7 mM for the heIF3b-RRM domain, with the heIF3j peptides added at a concentration of 0.7–1.0 mM in order to saturate the heIF3b-RRM domain with the long or short heIF3j peptide. All spectra were recorded at 25 °C.

Structure calculation

The structure of the heIF3b-RRM–heIF3j_{35–69} peptide complex was calculated using the program CYANA.⁴⁹ One thousand eight hundred fifty-three NOE-based distances derived from 3D heteronuclear NOESY experi-

ments, as well as 113 dihedral-angle restraints (ϕ and ψ) obtained by an analysis of N, H ^{α} , C ^{α} , and C ^{β} chemical shift values using the TALOS program,^{50,51} were used in structure calculations. Seven iterations for structural calculations and distance restraint assignment were run with CYANA. One hundred structures were calculated, and the 10 structures having the lowest energies were adopted. These structures were then water refined in a minimization run using the SANDER module of AMBER 9.0.⁵² The quality of each structure was assessed using the program PROCHECK-NMR.⁵³ A list of all restraints and structural statistics is presented in Table 1. Figures were prepared using the programs PyMOL[‡] and MOLMOL.⁵⁴

NMR structure determination of the heIF3b-RRM_{170–274}–heIF3j_{35–69} complex

The N-terminal heIF3j_{35–69} fragment of heIF3j displays the same binding mode as both full-length heIF3j and the larger N-terminal heIF3j_{1–69} peptide, displaying very similar chemical shift perturbations in heIF3b-RRM²⁰ (Supplementary Fig. 2a). More importantly, the same binding mode of both N-terminal heIF3j fragments was

[‡] <http://pymol.sourceforge.net/>

evidenced by virtually identical intermolecular NOEs of 11 residues surrounding Trp52 (Supplementary Fig. 2b). The structure of the complex was solved using 1916 experimental restraints that consist of 1853 distance restraints derived from NOE data, including 32 intermolecular NOEs extracted from isotope-filtered 2D and 3D experiments. In addition, 113 dihedral-angle restraints (ϕ and ψ angle restraints) were included from the analysis of $^{13}\text{C}/^{15}\text{N}$ chemical shifts using the program TALOS.⁵¹ Out of 100 calculated structures, the 10 lowest-energy structures having the best agreement with experimental restraints were subsequently refined in explicit solvent to improve the local geometry, electrostatics, and packing quality of the complex. Stereo views of the 10 lowest-energy structures (Supplementary Fig. 1) and structural statistics (Table 1) demonstrate a well-defined complex structure with low pairwise rmsd values of 1.19 ± 0.4 Å for heavy atoms, corresponding to residues 180–266 and 45–55 of hElF3b-RRM and hElF3j, respectively.

Preparation of human proteins

His-tagged hElF3b-RRM domain and hElF3j subunit were constructed as described previously²⁰ and transformed in *E. coli* BL21(DE3) cells. Cultures for hElF3b-RRM, hElF3j, and their mutants were grown at 37 °C, and protein overexpression was induced by addition of 1 mM IPTG at an A_{600} of 0.8. Cells were harvested 3 h after induction. For isotope labeling, minimal media containing $^{15}\text{NH}_4\text{Cl}$ and [^{13}C]glucose were used. All protein samples were purified over a nickel-chelating column (HiTrap; Amersham Biosciences), and this was followed by TEV protease cleavage for His-tag removal. The reaction mixture was then reloaded on a HiTrap chelating column charged with nickel sulfate to remove all of the TEV protease, the His tag, and minor contaminating proteins. After purification, the proteins were exchanged with appropriate buffer for subsequent experiments and further concentrated.

Preparation of hElF3j peptide

A DNA fragment encoding the hElF3j peptide sequence (residues 35–69) was prepared by PCR from full-length hElF3j plasmid DNA, digested with NdeI and EcoRI, and ligated into a modified pET28a vector (containing an N-terminal His₆ tag fused to a lipoyl domain,⁵⁵ followed by a TEV cleavage site and the standard pET28a multiple cloning site; Novagen) digested with the same enzymes. *E. coli* BL21(DE3) cells were transformed with the hElF3j peptide construct and grown at 37 °C in rich LB medium or minimal media containing $^{15}\text{NH}_4\text{Cl}$ and [^{13}C]glucose for production of unlabeled or labeled peptide, respectively. Protein overexpression was induced by addition of 1 mM IPTG at an A_{600} of 0.8. The hElF3j peptide fused to lipoyl domain was purified over a nickel-chelating column. TEV protease was then used to separate the hElF3j peptide from the lipoyl domain. Isolation of the hElF3j peptide required loading on a nickel-chelating column. This was followed by ion exchange (HiTrap DEAE; Amersham Biosciences) for further purification of the peptide.

ITC experiments

All calorimetric titrations were performed on a VP-ITC microcalorimeter (MicroCal). Protein samples were exten-

sively dialyzed against the ITC buffer containing 20 mM Hepes (pH 7.5) and 200 mM NaCl. All solutions were filtered using membrane filters (pore size, 0.2 μm) and thoroughly degassed for 20 min by gentle stirring under argon. The sample cell was filled with a 50 μM solution of full-length hElF3j wt or mutants and an injection syringe with 1 mM titrating hElF3b-RRM. Each titration typically consisted of a preliminary 2.5- μl injection, followed by 58 subsequent 5- μl injections every 210 s. All experiments were performed at 25 °C. Data for the preliminary injection, which are affected by diffusion of the solution from and into the injection syringe during the initial equilibration period, were discarded. Binding isotherms were generated by plotting heats of reaction normalized by moles of injectant *versus* the ratio of total injectant to total protein per injection. The data were fitted using Origin 7.0 (MicroCal).

Pull-down experiments

His₆-tagged hElF3b-RRM (wt and mutants) and untagged full-length hElF3j subunit were prepared as described above and buffer exchanged in equilibration buffer [50 mM sodium phosphate (pH 8) and 100 mM NaCl]. Each His₆-hElF3b-RRM construct was incubated with unlabeled hElF3j (final concentration of each protein, 30 μM) for 15 min at room temperature and loaded on His-select spin columns (Sigma) equilibrated with equilibration buffer. After two washing steps with equilibration buffer containing 5 mM imidazole, proteins were eluted with elution buffer [50 mM sodium phosphate (pH 8), 100 mM NaCl, and 250 mM imidazole]. The eluted proteins were resolved by denaturing gel electrophoresis and visualized by staining with Instant-Blue (Novexin). The percentage of hElF3j-bound fraction was evaluated by measuring band intensities with the NIH ImageJ program.

Accession number

The coordinates of the complex have been deposited into the Protein Data Bank under accession code 2KRB.

Acknowledgements

We are thankful to Alan G. Hinnebusch for critical reading of the manuscript; Jon R. Lorsch for communicating the results prior to publication; the members of the Valášek, Lukavsky, and Krásný laboratories for helpful comments; Ji-Chun Yang for assistance with NMR data collection; Andreas G. Tzakos for help with the structure calculation and expression of mutant proteins; and Olga Krydová and Ilona Krupičková for technical and administrative assistance. This research was supported by The Wellcome Trusts grant 076456/Z/05/Z, National Institutes of Health research grant R01 TW007271 funded by Fogarty International Center, Fellowship of Jan E. Purkyne from the Academy of Sciences of the Czech Republic, Institutional Research Concept AV0Z50200510 (to L.V.), and the Medical Research Council (to P.J.L.).

Supplementary Data

Supplementary data associated with this article can be found, in the online version, at [doi:10.1016/j.jmb.2009.12.047](https://doi.org/10.1016/j.jmb.2009.12.047)

References

- Hinnebusch, A. G., Dever, T. E. & Asano, K. A. (2007). Mechanism of translation initiation in the yeast *Saccharomyces cerevisiae*. In (Sonenberg, N., Mathews, M. & Hershey, J. W. B., eds), pp. 225–268, Cold Spring Harbor Laboratory Press, Cold Spring Harbor, NY.
- Pestova, T. V., Lorsch, J. R. & Hellen, C. U. T. (2007). The mechanism of translation initiation in eukaryotes. In (Sonenberg, N., Mathews, M. & Hershey, J. W. B., eds), pp. 87–128, Cold Spring Harbor Laboratory Press, Cold Spring Harbor, NY.
- Passmore, L. A., Schmeing, T. M., Maag, D., Applefield, D. J., Acker, M. G., Algire, M. A. *et al.* (2007). The eukaryotic translation initiation factors eIF1 and eIF1A induce an open conformation of the 40S ribosome. *Mol. Cell*, **26**, 41–50.
- Jivotovskaya, A., Valášek, L., Hinnebusch, A. G. & Nielsen, K. H. (2006). Eukaryotic translation initiation factor 3 (eIF3) and eIF2 can promote mRNA binding to 40S subunits independently of eIF4G in yeast. *Mol. Cell. Biol.* **26**, 1355–1372.
- Mitchell, S. F. & Lorsch, J. R. (2008). Should I stay or should I go? Eukaryotic translation initiation factors 1 and 1a control start codon recognition. *J. Biol. Chem.* **283**, 27345–27349.
- Valášek, L., Nielsen, K. H., Zhang, F., Fekete, C. A. & Hinnebusch, A. G. (2004). Interactions of eukaryotic translation initiation factor 3 (eIF3) subunit NIP1/c with eIF1 and eIF5 promote preinitiation complex assembly and regulate start codon selection. *Mol. Cell. Biol.* **24**, 9437–9455.
- Unbehaun, A., Borukhov, S. I., Hellen, C. U. & Pestova, T. V. (2004). Release of initiation factors from 48S complexes during ribosomal subunit joining and the link between establishment of codon–anticodon base-pairing and hydrolysis of eIF2-bound GTP. *Genes Dev.* **18**, 3078–3093.
- Szamecz, B., Rutkai, E., Cuchalova, L., Munzarova, V., Herrmannova, A., Nielsen, K. H. *et al.* (2008). eIF3a cooperates with sequences 5' of uORF1 to promote resumption of scanning by post-termination ribosomes for reinitiation on GCN4 mRNA. *Genes Dev.* **22**, 2414–2425.
- Hinnebusch, A. G. (2006). eIF3: a versatile scaffold for translation initiation complexes. *Trends Biochem. Sci.* **31**, 553–562.
- Valášek, L., Nielsen, K. H. & Hinnebusch, A. G. (2002). Direct eIF2–eIF3 contact in the multifactor complex is important for translation initiation *in vivo*. *EMBO J.* **21**, 5886–5898.
- Nielsen, K. H., Szamecz, B., Valasek, L., Jivotovskaya, A., Shin, B. S. & Hinnebusch, A. G. (2004). Functions of eIF3 downstream of 48S assembly impact AUG recognition and GCN4 translational control. *EMBO J.* **23**, 1166–1177.
- Nielsen, K. H., Valášek, L., Sykes, C., Jivotovskaya, A. & Hinnebusch, A. G. (2006). Interaction of the RNP1 motif in PRT1 with HCR1 promotes 40S binding of eukaryotic initiation factor 3 in yeast. *Mol. Cell. Biol.* **26**, 2984–2998.
- Yamamoto, Y., Singh, C. R., Marintchev, A., Hall, N. S., Hannig, E. M., Wagner, G. & Asano, K. (2005). The eukaryotic initiation factor (eIF) 5 HEAT domain mediates multifactor assembly and scanning with distinct interfaces to eIF1, eIF2, eIF3, and eIF4G. *Proc. Natl Acad. Sci. USA*, **102**, 16164–16169.
- Valášek, L., Mathew, A., Shin, B. S., Nielsen, K. H., Szamecz, B. & Hinnebusch, A. G. (2003). The yeast eIF3 subunits TIF32/a and NIP1/c and eIF5 Make critical connections with the 40S ribosome *in vivo*. *Genes Dev.* **17**, 786–799.
- Fraser, C. S., Berry, K. E., Hershey, J. W. & Doudna, J. A. (2007). 3j is located in the decoding center of the human 40S ribosomal subunit. *Mol. Cell*, **26**, 811–819.
- Spahn, C. M., Beckmann, R., Eswar, N., Penczek, P. A., Sali, A., Blobel, G. & Frank, J. (2001). Structure of the 80S ribosome from *Saccharomyces cerevisiae*—tRNA ribosome and subunit–subunit interactions. *Cell*, **107**, 373–386.
- Srivastava, S., Verschoor, A. & Frank, J. (1992). Eukaryotic initiation factor 3 does not prevent association through physical blockage of the ribosomal subunit–subunit interface. *J. Mol. Biol.* **220**, 301–304.
- Siridechadilok, B., Fraser, C. S., Hall, R. J., Doudna, J. A. & Nogales, E. (2005). Structural roles for human translation factor eIF3 in initiation of protein synthesis. *Science*, **310**, 1513–1515.
- Zhou, M., Sandercock, A. M., Fraser, C. S., Ridlova, G., Stephens, E., Schenauer, M. R. *et al.* (2008). Mass spectrometry reveals modularity and a complete subunit interaction map of the eukaryotic translation factor eIF3. *Proc. Natl Acad. Sci. USA*, **105**, 18139–18144.
- ElAntak, L., Tzakos, A. G., Locker, N. & Lukavsky, P. J. (2007). Structure of eIF3b RNA recognition motif and its interaction with eIF3j: structural insights into the recruitment of eIF3b to the 40S ribosomal subunit. *J. Biol. Chem.* **282**, 8165–8174.
- Methot, N., Rom, E., Olsen, H. & Sonenberg, N. (1997). The human homologue of the yeast Pti1 protein is an integral part of the eukaryotic initiation factor 3 complex and interacts with p170. *J. Biol. Chem.* **272**, 1110–1116.
- Fraser, C. S., Lee, J. Y., Mayeur, G. L., Bushell, M., Doudna, J. A. & Hershey, J. W. (2004). The j-subunit of human translation initiation factor eIF3 is required for the stable binding of eIF3 and its subcomplexes to 40S ribosomal subunits *in vitro*. *J. Biol. Chem.* **279**, 8946–8956.
- Asano, K., Phan, L., Anderson, J. & Hinnebusch, A. G. (1998). Complex formation by all five homologues of mammalian translation initiation factor 3 subunits from yeast *Saccharomyces cerevisiae*. *J. Biol. Chem.* **273**, 18573–18585.
- Phan, L., Zhang, X., Asano, K., Anderson, J., Vornlocher, H. P., Greenberg, J. R. *et al.* (1998). Identification of a translation initiation factor 3 (eIF3) core complex, conserved in yeast and mammals, that interacts with eIF5. *Mol. Cell. Biol.* **18**, 4935–4946.
- Valášek, L., Phan, L., Schoenfeld, L. W., Valášková, V. & Hinnebusch, A. G. (2001). Related eIF3 subunits TIF32 and HCR1 interact with an RNA recognition motif in PRT1 required for eIF3 integrity and ribosome binding. *EMBO J.* **20**, 891–904.
- Valášek, L., Hašek, J., Trachsel, H., Imre, E. M. & Ruis, H. (1999). The *Saccharomyces cerevisiae* HCR1 gene encoding a homologue of the p35 subunit of human translation eukaryotic initiation factor 3 (eIF3) is a high copy suppressor of a temperature-sensitive

- mutation in the Rpg1p subunit of yeast eIF3. *J. Biol. Chem.* **274**, 27567–27572.
27. Valášek, L., Hašek, J., Nielsen, K. H. & Hinnebusch, A. G. (2001). Dual function of eIF3j/Hcr1p in processing 20S pre-rRNA and translation initiation. *J. Biol. Chem.* **276**, 43351–43360.
 28. Kolupaeva, V. G., Unbehauen, A., Lomakin, I. B., Hellen, C. U. & Pestova, T. V. (2005). Binding of eukaryotic initiation factor 3 to ribosomal 40S subunits and its role in ribosomal dissociation and anti-association. *RNA*, **11**, 470–486.
 29. Valášek, L., Szamecz, B., Hinnebusch, A. G. & Nielsen, K. H. (2007). *In vivo* stabilization of preinitiation complexes by formaldehyde cross-linking. *Methods Enzymol.* **429**, 163–183.
 30. Fekete, C. A., Mitchell, S. F., Cherkasova, V. A., Applefield, D., Algire, M. A., Maag, D. *et al.* (2007). N- and C-terminal residues of eIF1A have opposing effects on the fidelity of start codon selection. *EMBO J.* **26**, 1602–1614.
 31. Hinnebusch, A. G. (2005). Translational regulation of GCN4 and the general amino acid control of yeast. *Annu. Rev. Microbiol.* **59**, 407–450.
 32. Grant, C. M., Miller, P. F. & Hinnebusch, A. G. (1994). Requirements for intercistronic distance and level of eIF-2 activity in reinitiation on GCN4 mRNA varies with the downstream cistron. *Mol. Cell. Biol.* **14**, 2616–2628.
 33. Clery, A., Blatter, M. & Allain, F. H. T. (2008). RNA recognition motifs: boring? Not quite.. *Curr. Opin. Struct. Biol.* **18**, 290–298.
 34. Nagai, K., Oubridge, C., Ito, N., Avis, J. & Evans, P. (1995). The RNP domain—a sequence-specific RNA-binding domain involved in processing and transport of RNA. *Trends Biochem. Sci.* **20**, 235–240.
 35. Pisarev, A. V., Hellen, C. U. T. & Pestova, T. V. (2007). Recycling of eukaryotic posttermination ribosomal complexes. *Cell*, **131**, 286–299.
 36. Isken, O., Kim, Y. K., Hosoda, N., Mayeur, G. L., Hershey, J. W. B. & Maquat, L. E. (2008). Upf1 phosphorylation triggers translational repression during nonsense-mediated mRNA decay. *Cell*, **133**, 314–327.
 37. Kielkopf, C. L., Lucke, S. & Green, M. R. (2004). U2AF homology motifs: protein recognition in the RRM world. *Genes Dev.* **18**, 1513–1526.
 38. Corsini, L., Bonnal, S., Basquin, J., Hothorn, M., Scheffzek, K., Valcarcel, J. & Sattler, M. (2007). U2AF-homology motif interactions are required for alternative splicing regulation by SPF45. *Nat. Struct. Mol. Biol.* **14**, 620–629.
 39. Selenko, P., Gregorovic, G., Sprangers, R., Stier, G., Rhani, Z., Kramer, A. & Sattler, M. (2003). Structural basis for the molecular recognition between human splicing factors U2AF(65) and SF1/mBBP. *Mol. Cell*, **11**, 965–976.
 40. Tabor, S. & Richardson, C. C. (1987). DNA sequence analysis with a modified bacteriophage T7 DNA polymerase. *Proc. Natl Acad. Sci. USA*, **84**, 4767–4771.
 41. Gietz, R. D. & Sugino, A. (1988). New yeast-*Escherichia coli* shuttle vectors constructed with *in vitro* mutagenized yeast genes lacking six-base pair restriction sites. *Gene*, **74**, 527–534.
 42. Sikorski, R. S. & Hieter, P. (1989). A system of shuttle vectors and yeast host strains designed for efficient manipulation of DNA in *Saccharomyces cerevisiae*. *Genetics*, **122**, 19–27.
 43. Smith, D. B. & Johnson, K. S. (1988). Single-step purification of polypeptides expressed in *Escherichia coli* as fusions with glutathione S-transferase. *Gene*, **67**, 31–40.
 44. Botstein, D., Falco, S. C., Stewart, S. E., Brennan, M., Scherer, S., Stinchcomb, D. T. *et al.* (1979). Sterile host yeasts (SHY): a eukaryotic system of biological containment for recombinant DNA experiments. *Gene*, **8**, 17–24.
 45. Asano, K., Clayton, J., Shalev, A. & Hinnebusch, A. G. (2000). A multifactor complex of eukaryotic initiation factors eIF1, eIF2, eIF3, eIF5, and initiator tRNA^{Met} is an important translation initiation intermediate *in vivo*. *Genes Dev.* **14**, 2534–2546.
 46. Mueller, P. P. & Hinnebusch, A. G. (1986). Multiple upstream AUG codons mediate translational control of GCN4. *Cell*, **45**, 201–207.
 47. Olsen, D. S., Savner, E. M., Mathew, A., Zhang, F., Krishnamoorthy, T., Phan, L. & Hinnebusch, A. G. (2003). Domains of eIF1A that mediate binding to eIF2, eIF3 and eIF5B and promote ternary complex recruitment *in vivo*. *EMBO J.* **22**, 193–204.
 48. Nielsen, K. H. & Valášek, L. (2007). *In vivo* deletion analysis of the architecture of a multi-protein complex of translation initiation factors. *Methods Enzymol.* **431**, 15–32.
 49. Guntert, P. (2004). Automated NMR structure calculation with CYANA. *Methods Mol. Biol.* **278**, 353–378.
 50. Cornilescu, G., Delaglio, F. & Bax, A. (1999). Protein backbone angle restraints from searching a database for chemical shift and sequence homology. *J. Biomol. NMR*, **13**, 289–302.
 51. Delaglio, F., Grzesiek, S., Vuister, G. W., Zhu, G., Pfeifer, J. & Bax, A. (1995). NMRPipe—a multidimensional spectral processing system based on Unix pipes. *J. Biomol. NMR*, **6**, 277–293.
 52. Case, D. A., Darden, T. A., Cheatham, T. E., Simmerling, C. L., Wang, J., Duke, R. E. *et al.* (2006). University of California, San Francisco, San Francisco, CA.
 53. Laskowski, R. A., Rullmann, J. A., MacArthur, M. W., Kaptein, R. & Thornton, J. M. (1996). AQUA and PROCHECK-NMR: programs for checking the quality of protein structures solved by NMR. *J. Biomol. NMR*, **8**, 477–486.
 54. Koradi, R., Billeter, M. & Wuthrich, K. (1996). MOLMOL: a program for display and analysis of macromolecular structures. *J. Mol. Graphics*, **14**, 51–55; 29–32.
 55. Dodd, R. B., Allen, M. D., Brown, S. E., Sanderson, C. M., Duncan, L. M., Lehner, P. J. *et al.* (2004). Solution structure of the Kaposi's sarcoma-associated herpesvirus K3 N-terminal domain reveals a novel E2-binding C₄HC₃-type RING domain. *J. Biol. Chem.* **279**, 53840–53847.